Alberto F. Maroto[1,2,3], Mireia Borrajo[1,2,3], Sílvia Prades[1], Àngela Callejo[4,5], Emilio Amilibia[4,5], Marta Pérez-Grau[4,5], Francesc Roca-Ribas[4,5], Elisabeth Castellanos[5,6], Alejandro Barrallo-Gimeno[1,2,3], Jordi Llorens[1,2,3]

The vestibular calyceal junction is dismantled in response to diverse injuring stimuli in rats and humans

[1] Departament de Ciències Fisiològiques, Universitat de Barcelona (UB), Feixa Llarga s/n, 08907 l'Hospitalet de Llobregat, Catalunya, Spain.

[2] Institut de Neurociències, Universitat de Barcelona (UB), Barcelona, Catalunya, Spain.

[3] Institut d'Investigació Biomèdica de Bellvitge (IDIBELL), 08907 l'Hospitalet de Llobregat, Catalunya, Spain.

[4] Servei d'Otorinolaringologia, Hospital Universitari Germans Trias i Pujol, Badalona, Catalunya, Spain.

[5] CSUR Phakomatoses Multidisciplinary Clinics HUGTIP-ICO-IGTP, Barcelona, Catalunya, Spain.

[6] Clinical Genomics Research Group, Institut de Recerca Germans Trias i Pujol (IGTP), Badalona, Catalunya, Spain.

Corresponding author: Prof. Jordi Llorens, Ph.D.; e-mail: jllorens@ub.edu; Ph: +34934024277

E-mail addresses and ORCID codes:

A.F.M.: albertomaroto@hotmail.com; 0000-0001-8265-4902

M.B.: mborrajoarjona@ub.edu; 0000-0003-2126-5713

19 S.P.: silvia.prab@gmail.com; 0000-0001-8561-2919

20 A.C.: angelacallejo@gmail.com; 0000-0003-3820-7405

21 E.A.: emilioamilibia@gmail.com; 0000-0003-0587-7891

22 M.P.G.: martaperezgrau@gmail.com; 0000-0003-4630-0116

23 F. R.R.: francescrocaribas@gmail.com; 0000-0001-6620-8216

24 E.C.: ecastellanos@igtp.cat; 0000-0002-8133-5325

25 A.B.G.: abarrallo@ub.edu; 0000-0003-2086-8926

26 J.L.: jllorens@ub.edu; 0000-0002-3894-9401

27 Acknowledgements

28 This study was supported by grant number RTI2018-096452-B-I00 and PID2021-124678OB-I00 (Ministerio de
29 Ciencia e Innovación, Agencia Estatal de Investigación, MCIU/AEI, 10.13039/501100011033, and European
30 Regional Development Fund, FEDER), grant number 2017SGR621 (Agència de Gestió d'Ajuts Universitaris i de
31 Recerca, AGAUR, Generalitat de Catalunya), and grant number 202007-30-31 (Fundació La Marató de TV3 2019)
32 . A.B.G is a Serra-Húnter fellow. The electron and confocal microscopy studies were performed at the Centres
33 Científics i Tecnològics de la UB (CCiTUB) of the Universitat de Barcelona. We thank Benjamín Torrejon-Escribano,
34 Rosa Rivera, Adriana Martínez Gené, Mora Gimeno, Josep Manel Rebled and Eva Prats for the expert and
35 technical help. We also thank Dr Bechara Kachar for the generous gift of the KCNQ4 antibody and Dr. Erin A.
36 Greguske for revision of the manuscript.

37

38 Competing interests

39 The authors declare no competing interests

ABSTRACT

Hair cell (HC) loss by epithelial extrusion has been described to occur in the rodent vestibular system during chronic 3,3'-iminodipropionitrile (IDPN) ototoxicity. This is preceded by dismantlement of the calyceal junction in the contact between type I HC (HCI) and calyx afferent terminals. Here, we evaluated whether these phenomena have wider significance. First, we studied rats receiving streptomycin for 3 to 8 weeks. Streptomycin caused loss of vestibular function associated with partial loss of HCI and decreased expression of CASPR1 (denoting calyceal junction dismantlement) in the calyces encasing the surviving HCI. Additional molecular and ultrastructural data supported the conclusion that HC-calyx detachment precede HCI loss by extrusion. Animals allowed to survive after the treatment showed functional recuperation and rebuilding of the calyceal junction. Second, we evaluated human sensory epithelia obtained during therapeutic labyrinthectomies and trans-labyrinthine tumour excisions. Some samples showed abnormal CASPR1 label strongly suggestive of calyceal junction dismantlement. Therefore, reversible dismantlement of the vestibular calyceal junction may be a common response triggered by chronic stress before HCI loss. This may partly explain clinical observations of reversion in function loss.

54 **INTRODUCTION**

55 Sensory encoding by the inner ear's vestibular system depends on the transducing function of hair cells (HC). In
56 most mammals, permanent loss of equilibrium and gaze control occurs as a result of HC loss considering that
57 these cells do not regenerate to a significant extent to restore functionality. Nevertheless, significant
58 recuperation in vestibular function is recorded clinically in a variety of disease conditions. In some cases, such as
59 benign paroxysmal positional vertigo (von Brevern et al., 2015), recuperation can be complete, suggesting that
60 the condition is associated with pathogenic mechanisms that transiently impair the system's function, but do
61 not cause HC loss. In other disease conditions, such as Ménière's disease (López-Escámez et al., 2015), recurrent
62 crises are often associated with incomplete recuperation and progressive worsening of the vestibular function.
63 In the case of exposure to ototoxic aminoglycoside antibiotics, irreversible loss of vestibular function is a
64 common outcome (Black et al., 2004), but significant yet incomplete recuperation has also been recorded (Black
65 et al., 2001). In recent years, we have used a sub-chronic ototoxicity model to identify reversible cellular and
66 molecular alterations in the vestibular epithelia that associate with reversible loss of vestibular function in rats
67 (Sedó-Cabezón et al., 2015) and mice (Greguske et al., 2019). These studies showed that the sub-chronic
68 ototoxic stress caused by the experimental compound 3,3'-iminodipropionitrile (IDPN) results in the
69 dismantlement of the calyceal junction between type I HCs (HCI) and the calyx afferent terminals, as
70 demonstrated by ultrastructural characterization and observed loss of the junction proteins CASPR1 (contactin-
71 associated protein) and tenascin-C, as well as delocalization of the voltage-gated potassium channel KCNQ4.
72 Simultaneously, the vestibular epithelium showed a loss of pre-synaptic and post-synaptic proteins, indicative of
73 synaptic uncoupling between the HCs and their afferents. These changes that are associated with the loss of
74 vestibular function are revealed by visible behavioural deficits. In this model, if the exposure was halted at an
75 early stage of the toxicity, both the epithelium alterations and the behavioural dysfunction were largely
76 reversible. In contrast, if the exposure was maintained, the functional loss persisted as a result of HC loss, which

77 predominantly occurred by the extrusion of live cells from the sensory epithelium into the endolymphatic cavity
78 (Llorens and Rodríguez-Farré, 1997; Seoane et al., 2001a,b; Sedó-Cabezón et al., 2015; Greguske et al., 2019).

79 The rat and mouse sub-chronic IDPN models illustrate a cellular pathway to HC demise that differs from
80 apoptosis (Seoane et al., 2001a). As explained in the previous paragraph, it concludes with the extrusion of HCs
81 after a phase of sensory cell detachment and synaptic uncoupling (Sedó-Cabezón et al., 2015; Greguske et al.,
82 2019). The fact that extrusion is the main form of HC demise in birds and amphibians following a variety of
83 insults (Hirose et al., 1999; Rubel et al., 2013), suggests that its molecular mechanisms may be highly conserved
84 across vertebrates and operate in response to diverse forms of damage. Surprisingly, this phenomenon has
85 received scarce attention and information is lacking about its molecular mechanisms and relevance to human
86 health. One first question worth addressing is whether these phenomena have a role in mammalian
87 aminoglycoside toxicity *in vivo*, as this is the main cause of vestibular toxicity in humans. Although most research
88 on aminoglycoside-induced HC loss has focused on apoptosis (Furness, 2015), the literature also contains
89 evidence that these drugs may cause vestibular HC extrusion (Li et al., 1995; Nakagawa et al., 1997; Granados
90 and Meza, 2005). In the present work, we studied whether dismantlement of the calyceal junction, synaptic
91 uncoupling, and HC extrusion occur in the rat vestibular epithelium in response to one aminoglycoside
92 antibiotic, streptomycin. Previously, we found that the mode of HC demise, whether extrusion, apoptosis, or
93 necrosis was determined by the intensity and duration of the toxic stress. Thus, high acute doses of IDPN caused
94 HC necrosis, sub-acute exposure to medium doses caused HC apoptosis and sub-chronic low dose exposure
95 elicited HC extrusion (Seoane et al., 2001a). These data indicate that short exposure paradigms aimed at
96 accelerating and synchronizing HC demise (Taylor et al., 2008; Oesterle et al., 2008; Benkafadar et al., 2021) may
97 in fact favour the apoptotic pathways above other possible pathways. Accordingly, for the present study we
98 investigated the effects of sub-chronic aminoglycoside exposure. As a second approach to evaluate the
99 relevance of these phenomena to human disease conditions, we explored their occurrence in the vestibular
100 epithelia of a substantial number of patients with vestibular schwannoma and a few with other vestibular

101 diseases that also require trans-labyrinthine tumour excision (meningioma and endolymphatic sac tumour) or
102 therapeutic labyrinthectomy (Ménière's disease). Vestibular schwannomas are tumours that grow in the
103 vestibular nerve and cause hearing and vestibular function loss. Current evidence indicates that this loss may in
104 part be caused by the negative impact pro-inflammatory factors secreted by the tumour have on the sensory
105 epithelia (Dilwali et al., 2015). The data we obtained demonstrate that calyceal junction dismantlement occurs
106 during chronic streptomycin toxicity in rats and provide evidence that it occurs in human vestibular epithelia in
107 response to other types of stress.

108 **RESULTS**

109 **Effects of streptomycin sulphate on body weight and overall health.**

110 To study the sub-chronic toxicity of streptomycin on the vestibular system, we administered male and female
111 rats with one daily dose of streptomycin sulphate (0, 100, 300, 400 or 500 mg/kg x day - groups CTRL, STR-100,
112 STR-300, STR-400, STR-500) for up to 6 or 8 weeks, starting at day 21 of age. Other groups of rats were
113 administered with two daily doses of 0, 300, 350 or 400 mg/kg - groups CTRL, STR-300x2, STR-350x2, STR-
114 400x2). Rats administered with streptomycin showed an acute sedative effect starting within a few minutes
115 after each daily dose, and was most evident in the group receiving the highest dose (STR-500): the animal stayed
116 quiet with decreased responsiveness and with an overtly low muscle tone. This effect usually lasted 15-20 min
117 but sometimes lasted for up to two hours after injection. During this sedation period, two rats died in the STR-
118 500 group on days 5 and 36, likely from respiratory arrest. Additionally, two rats died for unknown reasons after
119 days 20 and 37 in the STR-300 and STR-500 groups, respectively. No animals died when larger daily doses were
120 administered via two daily injections. Recuperation from this sedative effect was complete and surviving animals
121 showed normal behaviour except in regards to the evidences of vestibular dysfunction explained below. As
122 shown in Suppl. Fig. S1, streptomycin animals showed an increase in body weight at a smaller rate than that
123 shown by control rats. This resulted in significant differences in streptomycin versus control body weights after
124 five or more weeks of one daily dose, and by two weeks in the groups receiving two daily doses.

125 **Loss and recuperation of vestibular function after sub-chronic streptomycin exposure.**

126 Sub-chronic exposure to streptomycin sulphate caused a dose-dependent loss of vestibular function, as
127 indicated by the rat's abnormalities in spontaneous motor behaviour. Vestibular deficient animals showed
128 ataxia, spontaneous circling, and head bobbing. The loss of function was assessed using high-speed video
129 records of the tail-lift reflex as described (Martins-Lopes et al., 2019; Maroto et al., 2021a,c). A similar dose-
130 dependent effect occurred in male and female animals (Suppl. Fig. S2), and therefore animals of both sexes

131 were pooled for all further analyses. The decrease in tail-lift angles, indicative of loss of vestibular function, was
132 not significant in the STR-100 group, and smaller in the STR-300 and STR-400 groups compared to the STR-500
133 group (Suppl. Fig. S3), so further analysis on the one daily dose paradigm focused on this dose level. As shown in
134 Figure 1A, a progressive reduction in tail-lift angles was recorded in the STR-500 rats. Repeated-measures
135 MANOVA of the tail-lift data from days 0 (pre-test) to 42 resulted in significant day ($F[6,28]=15.38$, $p<0.001$),
136 treatment ($F[1,33]=18.0$, $p<0.001$), and day X treatment interaction ($F[6,28]=9.766$, $p<0.001$) effects, with
137 significant differences between CTRL and STR-500 mean values recorded at 4 to 6 weeks of exposure. Extension
138 of the administration up to 8 weeks caused only a modest additional effect on vestibular function (Suppl. Fig.
139 S4A).

140 By administering streptomycin in two daily injections, larger doses could be given to the animals and circumvent
141 the risk of death associated with the acute sedative effects of the drug. As shown in Fig. 1B, all the STR-300x2,
142 STR-350x2, and STR-400x2 groups showed faster and deeper loss of vestibular function than the STR-500 group.
143 MANOVA of the tail-lift data from the two daily injections experiment up to day 21 resulted in significant day
144 ($F[3,26]=191.1$, $p<0.001$), treatment ($F[3,28]=45.89$, $p<0.001$), and day X treatment interaction ($F[9,63.4]=20.92$,
145 $p<0.001$) effects. The effect was dose-dependent, and larger doses caused a faster progression of the decline in
146 vestibular function.

147 To evaluate the potential for functional recuperation, some animals were allowed to survive after the end of the
148 sub-chronic streptomycin exposure. As shown in Fig. 1C, rats exposed to 500 mg/kg · day of streptomycin for 6
149 weeks regained normal tail-lift angles during the recovery period. Functional recuperation was also observed in
150 the STR-500 rats exposed for 8 weeks (Suppl. Fig. S4B). The individual values of animals allowed to recover after
151 3 weeks of two daily doses of streptomycin also showed a clear recuperation of the tail-lift reflex (Fig. 1D).

152 **Sub-chronic streptomycin exposure caused partial loss of HCs in the vestibular sensory epithelia.**

153 To evaluate the major effects of streptomycin on the vestibule, we observed surface preparations of the sensory
154 epithelia using scanning electron microscopy (SEM). As reported in previous studies (Llorens et al., 1993; Seoane
155 et al., 2001a; Sedó-Cabezón et al., 2015), SEM observation of control epithelia (n=16) (Fig. 2A; Suppl. Fig. S5A, B)
156 revealed morphological features matching literature descriptions of healthy untreated rats with high densities of
157 stereocilia bundles. Epithelia from STR-300 animals (6 weeks of exposure, n=3) showed similar features to
158 control epithelia, except for indications of a few missing hair bundles or occasional bundles with fused
159 stereocilia (data not shown). For animals administered with larger doses of streptomycin once a day, the SEM
160 observations revealed scant to moderate loss of stereocilia bundles. Similar findings were obtained in STR-500
161 rats with small difference observed between animals exposed for 6 (n=6) or 8 (n=7) weeks, and in STR-400 rats
162 exposed for 8 weeks (n=2). Hair bundle loss was roughly similar in cristae (Suppl. Fig. S5C), utricles (Suppl. Fig.
163 S5D), and saccules (Fig 2B, C), with no evidence of an overt difference in susceptibility among receptors. In all
164 cases, the loss of stereocilia bundles was partial and many bundles were still present in the sensory receptors of
165 the worst cases (Suppl. Fig. S5E,F). In these SEM observations, images indicating ongoing damage were scarce.
166 Nevertheless, some evidence for fused stereocilia and HC protrusion were found (Fig 2D,E). Animals given two
167 daily injections of streptomycin displayed a larger loss of stereocilia bundles than the animals administered for
168 once a day (Suppl. Fig. S6). Evidence for ongoing damage was scarce in some epithelia, but clear in other
169 samples, including images of epithelial scars, bundle fusion, and cell protrusion towards the endolymphatic
170 cavity (Suppl. Fig. S6). The average extent of hair bundle loss was similar in STR-300x2 rats treated for 6 weeks
171 (n=7), STR-350x2 rats treated for 4 weeks (n=6), and STR-400x2 rats treated for 3 weeks (n=6).

172 To determine the loss of HCs revealed by the decreased densities of hair bundles observed by SEM in STR-500
173 rats, we obtained type I HC (HCI) and type II HC (HCII) counts from the vestibular epithelia of the other ear of the
174 same animals. To this end, we immunostained the epithelia with antibodies against myosin-7a (MYO7A),
175 CASPR1, and the calcium-binding protein calretinin, revealed by fluorescent secondary antibodies. In the
176 confocal microscopy images, HCI were identified as MYO7A+ cells (a pan-HC marker, Hasson et al., 1997)

177 surrounded by a CASPR1+ calyx (Sousa et al., 2009; Lysakowski et al., 2011; Sedó-Cabezón et al., 2015), even if
178 weak or fragmented, or with an unambiguous HCI shape with a long and narrow neck. As an estimate of HCII, we
179 counted cells with double MYO7A and calretinin label (Dechesne et al., 1991). The data obtained, presented in
180 Fig. 3A-C, reveal a significant decrease in HCI counts in both peripheral and central/striola regions of the crista
181 and the utricle and in the periphery of the saccule. ANOVA results were: central crista, $F[3,27]= 12.82$, $p<0.001$;
182 peripheral crista, $F[3,24]=2.89$, $p=0.056$; central utricle, $F[3,25]=23.86$, $p<0.001$; peripheral utricle,
183 $F[3,26]=44.95$, $p<0.001$; central saccule, $F[3,20]=2.01$, $p=0.15$ - N.S.; peripheral saccule, $F[3,22]=8.31$, $p=0.001$.
184 The most affected receptor was the utricle with a 52-67 % decrease in HCI counts in STR-500 animals, followed
185 by the crista, where a 30-40 % loss was recorded. In both the crista and the utricle, similar effects were recorded
186 in animals exposed for 6 weeks and animals exposed for 8 weeks. In the saccule, the loss was smaller than in the
187 crista and utricle receptors, and greater at 8 weeks than at 6 weeks of treatment. HCI counts remained reduced
188 in animals allowed to recover after the end of the exposure period, indicating an insignificant capacity for
189 regeneration. In contrast to HCI, no significant differences were obtained among treatment groups in HCII
190 counts (all p values > 0.1).

191 As explained above, the SEM observations indicated a loss of HC after two daily injections of streptomycin
192 greater than that recorded after one daily injection. To estimate HC loss according to cell type, we
193 immunostained crista receptors with antibodies against secreted phosphoprotein 1 (SPP1) / osteopontin,
194 CASPR1, and calretinin. HCI were identified by the SPP1 label (Burns et al., 2015; McInturff et al., 2018; Maroto
195 et al., 2021b), while the main population of HCII was identified by the calretinin+ label. As shown in Fig. 3D,E,
196 the number of HCI was greatly reduced after two daily injections of streptomycin ($F[4,26]=84.6$; $p<0.001$), while
197 the number of HCII was unchanged ($F[4,26]=1.45$, $p=0.25$). The loss of HCI was similar in the three groups of rats
198 treated with streptomycin (STR-300x2, STR-350x2, STR-400x2), and no recuperation in HCI counts was recorded
199 in the recovery group.

200 **Calyceal junction dismantlement, afferent fragmentation, and synaptic loss after sub-chronic streptomycin**
201 **exposure.**

202 In addition to HCl loss, rats exposed to sub-chronic streptomycin displayed alterations in the remaining HCIs and
203 their afferents. In rats exposed to streptomycin once a day (STR-500), a reversible loss of CASPR1 fluorescence
204 occurred in the calyces contacting the surviving HCIs (Fig.5). To assess this effect, we measured the amount of
205 CASPR1 fluorescence associated with the remaining individual calyces. The loss and recuperation of the CASPR1
206 label was found across the three epithelia and in both central/striolar and peripheral zones. All ANOVA
207 comparisons resulted in significant differences (all $F[3, 19 \text{ to } 27] > 5.3$, all $p's<0.006$). As shown in Fig. 4, the
208 confocal microscope images also revealed a reversible decrease in MYO7A fluorescence intensity in the HCs of
209 the STR-500 animals. This effect was quantified in a subset of samples and significant group differences were
210 found ($F[2,11]=5.0$, $p=0.029$). The post-hoc analysis confirmed that the label (in arbitrary units) was reduced
211 from 9583 $\pm$ 1290 ($X\pm SE$, n=5) in CTRL animals to 6232 $\pm$ 781 (n=4) in STR-500 (8 wk) animals ($p<0.05$, Duncan's
212 test), and regained normal level (10522 $\pm$ 621, n=5) after recovery. In animals given two injections a day, the
213 intensity of CASPR1 immunoreactivity in the calyces contacting surviving HCI was also reduced by streptomycin
214 (Suppl. Fig. S7).

215 We also evaluated whether sub-chronic streptomycin altered the distribution of the potassium channel, KCNQ4,
216 in the calyx membrane, as identified in CASP1-KO mice (Sousa et al., 2009) and in rats exposed to sub-chronic
217 IDPN (Sedó-Cabezón et al., 2015). The data, shown in Fig. 5A,B, indicated that CASPR1 loss is associated with
218 KCNQ4 redistribution in the calyces of the STR-500 rats. In control rats, the KCNQ4 label is found almost
219 exclusively in the inner membrane, that is, in the calyceal junction area, and is absent in the outer membrane of
220 the calyx. After streptomycin treatment, the immunofluorescence was reduced in the inner membrane, whereas
221 significant labelling appeared in the outer membrane of the calyx. Therefore, KCNQ4 was abnormally distributed
222 after streptomycin. ANOVA analyses of the amount of fluorescence in the inner and outer membranes were

223 significant ($F[3, 14]=12.1$, $P<0.001$, and $F[3,14]=49.9$, $p<0.001$, respectively). Post-hoc analyses confirmed that
224 streptomycin caused KCNQ4 redistribution, and that this effect was no longer present in the recovery animals.

225 Sub-chronic streptomycin also caused a reduction in the number of synaptic puncta as revealed by labelling with
226 antibodies against ribeye/CtBP2, the core protein of the presynaptic ribbon, and against the post-synaptic
227 scaffold protein PSD-95 (post-synaptic density 95). The mean number of puncta counts per cell in 2.7 μm thick
228 sections of HCs was significantly reduced in STR-500 animals exposed for 6 weeks compared to CTRL animals
229 (Fig. 5C,D). T-test comparisons resulted in $p <0.001$, $p=0.018$, and $p=0.001$ for ribeye, PSD-95, and co-localization
230 values, respectively.

231 The effect of sub-chronic streptomycin on the calyceal junction was also studied at the ultrastructural level by
232 TEM observation of samples from control rats (4 lateral crista, 2 saccules, 1 utricle), STR-500 rats exposed for 6
233 (5 lateral crista) or 8 (4 lateral crista) weeks, and STR-300x2 rats exposed for 6 weeks (3 saccules and 1 utricle).
234 In control specimens, calyceal junctions were prominent with virtually no disruptions in the two basal thirds of
235 contact between HCI and its afferent calyx (Fig. 6A,C). This junction consists of highly electron-dense pre- and
236 post-synaptic membranes, a highly regular inter-membrane distance, and an electron-dense extracellular space.
237 In contrast, many calyces in the streptomycin rats showed from fragmented to only partial to absent junctions
238 (Fig. 6B, D-F). In these units, the membrane density was similar to that of regular membranes and the area
239 displayed a more-variable inter-membrane distance, as well as a reduced extracellular electron density. In
240 addition, fragmented calyces were also identified in the samples from the treated animals, and these showed
241 absence of the calyceal junction (Fig. 6E, F). No fragmented calyces were observed in the control epithelia.

242 **Hair cell extrusion after sub-chronic streptomycin exposure.**

243 The occurrence of HC extrusion was evaluated by immunofluorescent analysis in samples from animals exposed
244 to streptomycin twice a day. The MYO7A and CASPR1 antibodies were combined with an anti-radixin antibody to
245 label the apical microvilli of the supporting cells and thus outline the surface of the epithelium. Images indicating

246 HC extrusion were not obtained in most sections of the crista (n=4 CTRL, 7 STR-300x2, 4 STR-350x2, and 4 STR-
247 400x2) and saccule (n=2 CTRL, 7 STR-300x2, 5 STR-350x2, and 6 STR-400x2). However, as illustrated in Fig. 7A,
248 protruding/extruding HCs were a common finding in most utricle sections from animals exposed to STR-300x2
249 for 6 weeks (n=7) or STR-350x2 for 4 weeks (n=5), although not in utricles from animals receiving STR-400x2 for
250 3 weeks (n=6). Control utricles (n=2) also showed no HC extrusion. In the STR-300x2 and STR-350x2 utricles, the
251 occurrence was around 1-3 protruding/extruding HC per section (130-190 μm long, 25 μm thick).

252 To corroborate that the extruding MYO7A+ profiles found in the immunofluorescent analyses corresponded to
253 living HCs, we examined two utricles by TEM. As shown in Fig. 7B,C, the extruding HC showed displacement of
254 the whole cell towards the lumen of the utricle. The ultrastructural features of the cytoplasm, organelles, and
255 nucleus indicated continued activity of the cell.

256 **Occurrence of calyceal junction dismantlement in human vestibular epithelia.**

257 To evaluate whether calyceal junction dismantlement also occurs in human vestibular epithelia under stress, we
258 studied samples from patients submitted to therapeutic labyrinthectomy or translabyrinthine tumour excision.
259 The vestibular epithelia were immunolabeled with anti-CASPR1 antibodies combined with a variety of other
260 antibodies, and a total of 29 samples yielded useful information. MYO7A, calretinin, and CASPR1 labels matched
261 the labelling features described above in rat samples. Also, when tested together (n=9), CASPR1 and the
262 extracellular matrix protein tenascin-C were found to localise together in the calyceal junction area, as described
263 previously in rodent samples (Lysakowski et al., 2011; Sedó-Cabezón et al., 2015; Greguske et al., 2019). In
264 contrast, the observed label of HCI by SPP1 was unreliable in the tested conditions. Among the 29 epithelia, HC
265 densities varied from high, similar to that observed in samples from control rats, to almost null. Reduced HC
266 density could result from both the patient's age and vestibular pathology; the evaluation of this pathology was
267 beyond the scope of the present study. Regarding the calyceal junctions, 18 samples were evaluated to have
268 intact or mostly intact CASPR1-labelled calyces. These included 2/2 cases of Ménière's Disease (Fig. 8A), 4/4

269 cases of meningioma (Fig. 8B,C), 1/1 case of an endolymphatic sac tumour, and 11/22 cases of vestibular
270 schwannoma. Two other samples displayed very few HCs with only one CASPR1+ or none, hampering the
271 achievement of any conclusion on calyceal junctions. However, 9 of the samples, all of them from vestibular
272 schwannoma patients, provided images suggesting that an active process of calyceal junction dismantlement
273 was taking place. This included calyces with patched CASPR1 labelling (Fig 8D-F) or lack of CASPR1 in calyx-only
274 units (Fig. 8G). The patched feature of the label in some calyces was confirmed in 3D reconstructions (Suppl. Fig.
275 S8). The number of days the samples were in fixative does not explain this effect, as it was observed in tissues
276 fixed for 1 day (n=5), 4 days (n=1), 7 days (n=1), and unrecorded (but less than 8) days (n=2).

277 **DISCUSSION**

278 Previous work from our laboratory in rats and mice has demonstrated that sub-chronic IDPN exposure causes
279 vestibular HC extrusion and that the extrusion is preceded by reversible calyceal junction dismantlement and
280 synaptic uncoupling (Seoane et al., 2001a; Sedó-Cabezón et al., 2015; Greguske et al., 2019). These phenomena
281 have received little research attention despite its potential relevance. HC extrusion is the main form of HC
282 demise in birds and amphibians (Hirose et al., 1999; Rubel et al., 2013) and has been sporadically observed in
283 mammalian vestibular epithelia (Li et al., 1995; Nakagawa et al., 1997; Granados and Meza, 2005). In the present
284 work, we first aimed at establishing a new rat model of sub-chronic aminoglycoside toxicity to determine
285 whether HC detachment and extrusion occur in ototoxic conditions of clinical relevance. The data obtained
286 demonstrate that the calyceal junction reversibly dismantles during subchronic streptomycin exposure in
287 association with reversible vestibular dysfunction. Synaptic uncoupling and HC extrusion were also recorded in
288 these rats. In addition, we also collected evidence indicating that calyceal junction dismantlement may take
289 place in the human vestibular system.

290 HC degeneration is effectively achieved by direct exposure to aminoglycoside antibiotics as done by trans-
291 tympanic administration or in *in vitro* studies (Kohonen and Tarkkanen, 1969; Anniko et al., 1982). However, the
292 use of more natural *in vivo* approaches to induce inner ear toxicity in laboratory animals with aminoglycosides
293 has been a challenging issue, as acute systemic intoxication may not cause ototoxic effects until the dose is large
294 enough to trigger animal death (Wu et al., 2001; Murillo-Cuesta et al., 2010). Nevertheless, several studies have
295 succeeded in establishing dosing regimes that elicit ototoxic effects with limited lethality and systemic toxicity.
296 Yet, many of these studies favour cochlear versus vestibular toxicity (Sullivan et al., 1987) or are designed to
297 accelerate the progression of the damage (Taylor et al., 2008; Oesterle et al., 2008). In the present study, we
298 successfully caused slowly progressing vestibular toxicity with streptomycin in young rats. By means of one daily
299 injection, significant loss of vestibular function occurred after four weeks of the highest tolerated dose, while
300 the use of two injections per day accelerated this loss in a dose-dependent manner, allowing for the study of

301 ototoxicity emerging after 2-3 weeks of treatment. Interestingly, the effects were similar in both sexes and low
302 variability was recorded within groups. Thus, as similarly reported for cochlear kanamycin toxicity in rats and
303 mice (Wu et al., 2001; Jiang et al., 2006), exposure of Long-Evans rats to one or two daily doses of streptomycin
304 reliably causes vestibular toxicity. Comparing the two models, it appears that the one daily dose regimen
305 reaches a limit in its effect, while the two-dose regimen seems to provide a more flexible model to study dose-
306 and time-dependent effects.

307 Streptomycin exposure in rats caused the loss of HCs, deeper after two daily doses than after one dose, as
308 revealed by the SEM studies and quantified in immunofluorescence studies. Separate counts of HCI and HCII
309 revealed that HC loss concentrated on the HCI, while HCII were spared in both injection paradigms. To identify
310 HCI we used two different markers, CASPR1 and SPP1. CASPR1 is not expressed by HCIs but is found in the
311 membrane of the calyx afferent contacting the HCI (Sousa et al., 2009; Lysakowski et al., 2011; Sedó-Cabezón et
312 al., 2015). Although streptomycin caused a specific loss of CASPR1, traces of CASPR1 label in contact with cell
313 profiles positive for Myo7a+ and negative for calretinin (see Fig 3A) allowed a reliable identification of HCI in the
314 one dose samples. Also, except for a minor recuperation in HCI numbers in the periphery of utricles and cristae,
315 no increase in HCI numbers was found in the samples of the recovery animals, in which a good recuperation in
316 CASPR1 expression had occurred. In addition, the loss of HCI was confirmed using a positive HCI marker, SPP1
317 (McInturff et al., 2018), to evaluate the samples from the two daily injections experiment. To identify HCII, we
318 also used a positive marker, calretinin, and found that the number of HCII per image was not reduced in any of
319 the two exposure paradigms. Because of the method used, we cannot completely exclude that a small loss of
320 HCII was masked by tissue shrinkage, but in any case the lack of differences in HCII numbers per image contrasts
321 with the significant loss of HCI. While a greater sensitivity of HCI with respect to HCII in regards to ototoxic insult
322 is widely recognized, not many studies are available in providing a quantitative assessment of this difference *in*
323 *vivo* (Lopez et al., 1997; Nakayama et al., 1996 ; Hirvonen et al., 2005; Maroto et al., 2021a).

324 The data collected add to the existing evidence that HC extrusion is a significant form of HC demise induced by
325 aminoglycosides in the mammalian vestibular system *in vivo*, as reported in the vestibular epithelia of rodents
326 exposed to other aminoglycosides using relatively long exposure paradigms (Li et al., 1995; Granados and Meza,
327 2005). Also, the present data demonstrate that calyceal junction dismantlement and synaptic uncoupling occur
328 after streptomycin, as previously demonstrated for sub-chronic IDPN (Sedó-Cabezón et al., 2015; Greguske et
329 al., 2019). The streptomycin effect includes CASPR1 down-regulation, redistribution of KCNQ4, loss of electron
330 density in the calyceal junction area, and a reduction in the number of synaptic puncta per cell. As observed in
331 the IDPN model, these effects are associated with the loss of vestibular function, and significant recuperation
332 was also recorded for the behavioural, CASPR1, and KCNQ4 effects in rats when allowed a recovery period after
333 the exposure. However, significant differences between the two models were noticed. In the rat IDPN model
334 (Seoane et al., 2001a; Sedó-Cabezón et al., 2015), a complete dismantlement of the calyceal junctions, with
335 extensive loss of CASPR1 and redistribution of KCNQ4 occurs before HC loss starts. Extending the time of IDPN
336 exposure triggers a massive event of HC extrusion, and the occurrence of extruding cells over several weeks
337 indicates that the extrusion of each HC takes place over several days. IDPN thus provides a highly synchronic and
338 slowly progressing model of sequential HC detachment and extrusion. In contrast, in the streptomycin rats,
339 extruding HC were only found occasionally, the loss of CASPR1 and the redistribution of KCNQ4 were smaller,
340 and a significant loss of HCs had occurred already before complete dismantlement of the calyceal junctions.
341 These observations indicate that, in comparison to those of IDPN, the effects of streptomycin are less
342 synchronic, and that the extrusion of each HC takes place in a shorter time, probably a few hours. Although not
343 specifically addressed in the present experiments, the TEM studies did not give evidence for an extensive
344 occurrence of apoptotic HC death. The simplest explanation of the present observations is that HC detachment
345 and extrusion are triggered at the individual cell level, and that cells are not synchronized after streptomycin
346 treatment as they are after IDPN. This conclusion is supported by our previous demonstration that calyceal

347 junction dismantlement is triggered individually in a calyx-to-calyx basis also after IDPN (Sedó-Cabezón et al.,
348 2015).

349 Behavioural and CASPR1 data presented here demonstrate repair capacity and functional recuperation of the rat
350 vestibular epithelium after sub-chronic streptomycin exposure. Although only a limited number of animals were
351 allowed to survive, their recuperation was indubitable. Functional recuperation may be a consequence of
352 behavioural compensation or reflect recuperation from alterations not detected by histological analyses, such as
353 hypothetical changes in endolymph composition or inactivation of the transduction channels. Conversely, our
354 data excluded the possibility that HC regeneration accounted for this recuperation, because HCI counts
355 remained decreased at the end of the recovery period. Rather, its association with the reversal in CASPR1
356 labelling, as measured on a cell-by-cell basis, suggests that the functional recuperation may result, at least in
357 part, from repair phenomena in the HC and the contact between HCs and their afferents. The present
358 observation of a recuperation in CASPR1 labelling contradicts the persistence of calyceal pathology observed in
359 chinchillas exposed to gentamicin by direct perilymphatic infusion (Sultemeier and Hoffman, 2017). Differences
360 in species, aminoglycosides, and exposure model may account for the difference between the present data and
361 those by Sultemeier and Hoffman (2017).

362 To explore the possible relevance of the calyceal junction dismantlement to human pathology, we examined a
363 series of human samples for histological evidence of such dismantlement. The interpretation of the human
364 observations is weakened by the lack of control samples, and the variability in pathological conditions and
365 surgery-generated damages. Nevertheless, many samples included a uniform CASPR1 label in all observable
366 calyces, while some other samples offered multiple images of patched or largely missing label for this protein.
367 Although the possibility that this abnormality was generated during collection of the sample cannot be
368 completely excluded, the data strongly suggest that calyceal junction dismantlement may indeed occur in the
369 human vestibule under stressful conditions. Although all the cases in which CASPR1 loss was recorded were
370 from vestibular schwannoma surgeries, the number of samples from other pathologies was so low that it cannot

371 be discarded that similar observations could emerge if more cases were examined. Current evidence indicates
372 that vestibular schwannomas may damage the sensory epithelia of the inner ear through tumour-secreted
373 factors, including tumour necrosis factor alpha (TNFα) (Dilwali et al., 2015). A recent study has demonstrated
374 the potential of this pro-inflammatory cytokine to cause cochlear synaptic uncoupling *in vivo* (Katsumi et al.,
375 2020). It is thus possible that inflammatory signals like TNFα are able to trigger the dismantlement of the
376 calyceal junction, synaptic uncoupling, and eventual HC extrusion in the vestibular epithelium.

377 Future work may address some of the limitations of this initiating study and use it to expand our understanding
378 of vestibular pathophysiology. For instance, determining the blood and inner ear concentrations of streptomycin
379 (and its potential ototoxic metabolites, e.g. Granados and Meza, 2005) in this exposure model may enlighten the
380 role of inner ear accumulation in systemic aminoglycoside toxicity. Recent data supports that cochlear retention
381 is a key factor in cisplatin ototoxicity (Breglio et al., 2017), and some data is available supporting a similar
382 conclusion for the cochlear and vestibular toxicity of gentamicin (Imamura and Adams, 2003). More works is
383 also needed to replicate and expand the human observations, excluding any potential confounding factor and
384 relating the pathological findings to the clinical data of patients. This is particularly important due to the lack of
385 tissues from humans not suffering any inner ear disease.

386 In conclusion, the present study evaluated whether events leading to HC extrusion in the vestibular sensory
387 epithelia of rodents exposed to sub-chronic IDPN (Seoane et al., 2001a; Sedó-Cabezón et al., 2015; Greguske et
388 al., 2019) may have a wider significance. The data collected demonstrate that dismantlement of the calyceal
389 junction and synaptic uncoupling are widespread phenomena in rats exposed to sub-chronic streptomycin
390 regimes that cause HC loss through, at least in part, the extrusion pathway. We also collected data suggesting
391 that calyceal junction dismantlement may occur in human vestibular epithelia in response to inflammatory
392 stress. Elucidating the molecular pathways triggering these cellular phenomena may unveil new targets to
393 control damage progression in this sensory epithelium.

394 **MATERIALS AND METHODS**

395 **Animals and treatments**

396 Animals were used in accordance with Law 5/1995 and Act 214/1997 of the Generalitat de Catalunya and
397 approved by the University of Barcelona's Ethics Committee on Animal Experiments and the Commission on
398 Animal Experimentation of the Generalitat. Long-Evans rats were obtained from Janvier Labs (Le-Genest-Saint-
399 Isle, France) at post-natal day 8-12. They were housed with lactating mothers in standard Macrolon cages
400 (215×465×145 mm) with wood shavings as bedding. At day 21, the rats were weaned and housed in groups of
401 four of the same sex. Housing conditions included a 12:12 h light:dark cycle (07:30-19:30 h), a 22±2°C room
402 temperature and an *ad libitum* access to standard pellet diets (TEKLAD 2014, Harlan Laboratories, Sant Feliu de
403 Codines, Spain).

404 A total of 98 rats (58 males, 40 females) were used in two different administration protocols, one injection per
405 day and two injections per day. The first administration protocol was designed on the grounds of the protocols
406 by Granados and Meza, 2005, and Schirmer et al., 2007. Animals were administered streptomycin sulphate salt
407 (Sigma-Aldrich, S6501), s.c., dissolved in PBS, starting at postnatal 21, daily for 6 or 8 weeks. To ensure dose
408 accuracy, injection volumes were 10 ml/kg at the beginning, but were reduced to 2 ml/kg as the rats increased
409 body weights. Different injection sites in the dorsal skin were used in an alternating sequence. In this first series
410 of experiments, rats were dosed with 0 (control vehicle), 100, 300, 400 or 500 mg/kg · day of streptomycin
411 (referred to the free base), once a day, for 6 or 8 weeks. Two experimental batches used only males, one of
412 them used only females, and the fourth one included an equal number of males and females. Acute toxicity and
413 lethality is described in the results section above. A final experiment used a second administration protocol, in
414 which the total daily dose was split into two injections given 8 h apart. This dosing paradigm was designed to
415 evaluate the vestibular effects of larger daily doses and circumvent the acute toxicity of streptomycin recorded
416 in rats receiving the 500 mg/kg dose. Thus, rats received 0, 600, 700 or 800 mg/kg · day in two daily doses of 0,

417 300 mg/kg (for 6 weeks), 350 mg/kg (for 4 weeks) or 400 mg/kg (for 3 weeks). No animals died in this
418 experiment. The detail of all groups of animals used is shown in Supplementary Table S1.

419 During the period of treatment, the animals were weighted and assessed for wellbeing daily. They were also
420 tested for vestibular function once a week. At the end of the treatment period, some animals were allowed to
421 survive for up to 8-10 additional weeks to evaluate the potential reversibility of the vestibular dysfunction and
422 the histopathological effects of streptomycin. Some control animals were also allowed to survive the recovery
423 period to provide control body weight and vestibular function data. The day after that of the last dose, or after
424 the recovery period, rats were euthanized by decapitation under anaesthesia. The skull was sectioned in half
425 and placed in fixative solution under a fume hood for dissection of the vestibular sensory epithelia. The epithelia
426 from the first ear were typically obtained within 5 min after decapitation and used for scanning (SEM) and
427 transmission (TEM) electron microscopy. The epithelia from the second ear, obtained within 15 min after
428 decapitation, were used for immunohistochemistry. Epithelia from some animals were used for
429 immunohistochemical analysis only. The numbers of animals used in each histological analysis are indicated in
430 the figures and are summarized in Suppl. Table S2.

431 **Human samples**

432 Vestibular sensory epithelia were collected from patients submitted to therapeutic labyrinthectomy or
433 translabyrinthine tumour excision. The samples included in the study, detailed in Suppl. Table S3, are from 2
434 cases of Ménière's Disease, 1 case of endolymphatic sac tumour, 4 cases of meningioma, and 22 cases of
435 vestibular schwannoma. Patients were 18 to 70 years old, and 52 % were females. The tissues were obtained
436 after informed consent, as approved by the Clinical Ethics Committee of the Hospital Germans Trias i Pujol. The
437 samples were immediately placed in 4% formaldehyde with <2.5% methanol (BiopSafe) and sent to the
438 laboratory, usually in 24 h, although some samples were delayed for up to 7 days (Suppl. Table S3). The tissues

439 were then rinsed in phosphate buffered saline (PBS, pH 7.2), transferred into a cryoprotective solution (34.5%
440 glycerol, 30% ethylene glycol, 20% PBS, 15.5% distilled water) and stored at -20ºC until further processing.

441 **Assessment of vestibular function in rats**

442 To evaluate vestibular function, we assessed the tail-lift reflex as described (Martins-Lopes et al., 2019; Maroto
443 et al., 2021 a,c). Briefly, rats are held by the base of the tail and quickly but gently lifted upwards to
444 approximately 40 cm above ground and immediately returned down. In healthy rats, this triggers a trunk and
445 limbs extension reflex in a landing response. Loss of vestibular function results in loss of the anti-gravity
446 extension reflex, so the rat curls ventrally (Hunt et al., 1987; Pellis et al., 1991; Llorens et al., 1993; Maroto et al.,
447 2021c). The reflex response of the animal is recorded from the side with high-speed video (we use 240 frames
448 per second with a GoPro 5 camera) and the records are used to obtain the minimum angle formed by the nose,
449 the back of the neck and the base of the tail during the tail-lift manoeuvre (tail-lift angle, TLA), as described
450 (Martins-Lopes et al., 2019; Maroto et al., 2021a,c). The TLA has been demonstrated to provide an objective
451 measure of permanent or reversible vestibular loss (Martins-Lopes et al., 2019; Maroto et al., 2021a,c).

452 **Electron microscopy**

453 For SEM and TEM, rat vestibular epithelia were dissected in 2.5% glutaraldehyde in 0.1 M cacodylate buffer (pH
454 7.2), and fixed overnight in this solution. The epithelia were then rinsed with cacodylate buffer, post-fixed for 1
455 h in 1% osmium tetroxide in the same buffer, rinsed again and stored in 70% ethanol at 4ºC until further
456 processing. Afterwards, the samples were dehydrated with increasing concentrations of ethanol, up to 100%.
457 For TEM analysis, the lateral crista was embedded in Spurr resin. To select the level of interest, semi-thin
458 sections (1 µm) were stained with 1% toluidine blue and examined in a light microscope. Ultrathin sections were
459 stained with uranyl acetate and lead citrate and were observed with a JEOL 1010 microscope at 75-80 kV. For
460 SEM analysis of epithelial surfaces, the dehydrated specimens were dried in a Polaron E3000 critical-point dryer
461 using liquid CO2, coated with carbon, and observed in a JEOL JSM-7001F field emission SEM.

462 **Immunohistochemistry**

463 The following commercial primary antibodies were used: mouse monoclonal anti-CASPR1 (clone K65/35, RRID:
464 AB_2083496, used at 1:400 dilution) and anti-PSD95 (clone K28/43, RRID: AB_2292909, 1:100) from the UC
465 Davis / NIH NeuroMab Facility; mouse monoclonal anti-Ribeye/CtBP2 (clone 16/CtBP2, BD Transduction Labs,
466 RRID: AB_399431, 1:100); rabbit anti-myosin VIIa (25-6790, Proteus Biosciences, RRID: AB_10015251; 1:400);
467 guinea pig anti-calretinin (214.104, Synaptic Systems, RRID: AB_10635160, 1/500); goat anti-SPP1 (AF808, RD
468 systems, RRID: AB_2194992, 1/200). We also used a rabbit anti-KCNQ4 (PB-180, 1/1000) donated by Bechara
469 Kachar (National Institute on Deafness and Other Communication Disorders, NIH; Beisel et al., 2005). To reveal
470 the primary antibodies, we used Day-Light-405, Alex-488, Alexa-555 and Alexa-647-conjugated secondary
471 antibodies from Invitrogen / Thermo Fisher. To image synaptic puncta, we used isotype-specific secondary
472 antibodies, i.e., anti-mouse-IgG1 to reveal the Ribeye/CtBP2 antibody and anti-mouse IgG2a to reveal the PSD-
473 95 antibody.

474 After dissection, the rat vestibular epithelia were fixed for 1 h at room temperature in 4 % paraformaldehyde in
475 PBS. These samples were rinsed in PBS, transferred into the cryoprotective solution and stored at -20ºC. To
476 circumvent potential bias from batch-to-batch differences in immunolabelling, we processed in parallel
477 specimens from each experimental group. For immunolabelling, rat or human tissues were washed with PBS to
478 remove the cryoprotective solution, permeated in 4% Triton-X-100 in PBS for 1 h at room temperature, and then
479 blocked in 0.5% Triton-X-100 and 1% fish gelatine in PBS (Sigma-Aldrich, cat.# G7765) also for 1 h at room
480 temperature. They were then incubated with the mixed primary antibodies in 0.1% Triton-X-100 and 1% fish
481 gelatine in PBS for 24 h at 4ºC, followed by incubation with the secondary antibodies in the same conditions.
482 The samples were thoroughly rinsed with PBS following each incubation and gently rocked during the
483 incubations and washes. The immunolabelled human epithelia were whole-mounted in Mowiol medium,
484 whereas the rat epithelia were sectioned before mounting in the same medium. To obtain sections, the tissues
485 were embedded in a mixture of 0.49% gelatin, 30% bovine serum albumin, and 20% sucrose in PBS overnight at

486 4 ºC. This same medium was used to form a block by solidification with 2 % glutaraldehyde, one sample placed
487 oriented in its surface, and a second block formed on top of it. Using a Leica VT1000S vibrating microtome,
488 sections of 40 μm were obtained from this layered block with the specimen placed in between the two halves. A
489 detailed version of this protocol has been published (Maroto et al., 2021b).

490 **Confocal microscopy observation and analysis**

491 Tissue sections were observed in a Zeiss LSM880 spectral confocal microscope. In animal studies, image
492 acquisition settings were maintained across samples from each immunolabelling batch. To obtain HC counts, Z-
493 stacks of optical sections were obtained each 0.5 μm spanning 25 μm with the 63X objective. Then, we obtained
494 8 sequential images (3 μm thick each) by the maximum intensity projection of 6 consecutive images from the
495 original stack. The ImageJ software (National Institute of Mental Health, Bethesda, Maryland, USA) was used for
496 quantitative image analyses. Epithelia of animals injected once a day with streptomycin were labelled with anti-
497 MYO7A, anti-CASPR1, and anti-calretinin antibodies. HCI were defined as MYO7A+ cells surrounded by a calyceal
498 CASPR1+ label, even in cases where this label appeared thin and fragmented, or cells with an unambiguous HCI
499 shape with a long and narrow neck. HCII were defined as cells labelled with both the anti-MYO7A and anti-
500 calretinin antibodies. MYO7A+ cells not identified as HCI or HCII (3-6 %) were excluded from the analysis. For
501 each animal and epithelial zone, the number of HCI and HCII per image was obtained by averaging counts from
502 the 8 images of a representative histological section. The histological sections used for counting were obtained
503 from similar locations in all animals. To evaluate the loss of CASPR1 label in the calyces, the amount of
504 fluorescence in the corresponding colour channel was measures in individual calyces using a 100 μm^2 region of
505 interest on a single optical section. For each animal, epithelium and zone, the average amount of fluorescence
506 was obtained from all HCs available for analysis up to 40 cells. Data were normalized as percentage of the mean
507 fluorescent intensity of control samples in the same batch of immunohistochemical processing and confocal
508 imaging. Then, statistical analyses were performed to compare among groups of animals. To compare the

509 distribution of KCNQ4 in the inner and outer membranes of the calyx, we assessed the profile of fluorescence
510 intensity along a line drawn across the calyx as described (Sousa et al., 2009; Sedó-Cabezón et al., 2015). Peak
511 fluorescence values were obtained for the inner and outer membrane of all calyces included in one
512 representative section of the epithelium, and average values were obtained per animal. To count synaptic
513 puncta, we imaged the tissues at 0.3 μm intervals to obtain Z-stacks of 2.7 μm. Only HC with their nuclei
514 extending top to bottom of the stack were used for counting, so the counts obtained were from a thick slice
515 from the middle region of the cell, not the whole cell. We counted presynaptic Ribeye/CtBP2 puncta,
516 postsynaptic PSD95 puncta, and pairs of Ribeye and PSD95 puncta that overlapped or were closely apposed (co-
517 localization). For each animal, average counts were obtained from a minimum of 30 HC.

518 Human samples were observed as whole mounts. The tissues were completely examined with the 40X and 63X
519 objectives. Representative Z-stacks, encompassing the entire thickness of the sensory epithelium, were obtained
520 from both striola and peripheral regions. The full stacks were thoroughly studied to determine the presence of
521 pathological features. This included colour channel splitting and merging, observation at several different
522 contrast and brightness adjustments, 3D reconstructions, maximum intensity projection of stacks or sub-stacks
523 and orthogonal projections. Images in Fig. 10 were prepared for illustration purposes only.

524 **Data analysis**

525 Data show mean +/- standard error of the mean except where indicated. Body weight and behavioural data
526 were analysed with repeated-measures MANOVA (Wilks' criterion) with the day as the within-subject factor.
527 Day-by-day analysis was performed after significant day-by treatment interactions were recorded. Other data
528 were analysed by appropriate ANOVA designs and Duncan's post-hoc test, or by Student's t-test. The IBM SPSS
529 Statistics 25 program package was used.

530 **REFERENCES**

531 Anniko, M., Takada, A. and Schacht, J. (1982) Comparative ototoxicities of gentamicin and netilmicin in three
532 model systems. *Am. J. Otolaryngol.* 3, 422-33.

533 Beisel, K.W., Rocha-Sanchez, S.M., Morris, K.A., Nie, L., Feng, F., Kachar, B., Yamoah, E.N. and Fritzsch, B (2005)
534 Differential expression of KCNQ4 in inner hair cells and sensory neurons is the basis of progressive high-
535 frequency hearing loss. *J. Neurosci.* 25, 9285–9293.

536 Benkafadar, N., Janesick, A., Scheibinger, M., Ling, A. H., Jan, T. A. and Heller, S. (2021). Transcriptomic
537 characterization of dying hair cells in the avian cochlea. *Cell Rep.* 34, 108902. doi:
538 10.1016/j.celrep.2021.108902

539 Black, F.O., Gianna-Poulin, C. and Pesznecker, S.C. (2001). Recovery from vestibular ototoxicity. *Otol. Neurotol.*
540 22, 662-671.

541 Black, F.O., Pesznecker, S. and Stallings, V. (2004). Permanent gentamicin vestibulotoxicity. *Otol. Neurotol.* 25,
542 559-569.

543 Breglio, A. M., Rusheen, A. E., Shide, E. D., Fernandez, K. A., Spielbauer, K. K., McLachlin, K. M., Hall, M. D.,
544 Amable, L. and Cunningham, L. L. (2017). Cisplatin is retained in the cochlea indefinitely following
545 chemotherapy. *Nat. Commun.* 8, 1654.

546 Burns, J. C., Kelly, M. C., Hoa, M., Morell, R. J. and Kelley, M. W. (2015). Single-cell RNA-Seq resolves cellular
547 complexity in sensory organs from the neonatal inner ear. *Nat. Commun.* 6, 8557. doi:
548 10.1038/ncomms9557

549 Dechesne, C.J., Winsky, L., Kim, H.N., Goping, G., Vu, T.D., Wenthold, R.J. and Jacobowitz, D.M. (1991)
550 Identification and ultrastructural localization of a calretinin-like calcium-binding protein (protein 10) in the
551 guinea pig and rat inner ear. *Brain. Res.* 560, 139-148.

552 Dilwali, S., Landegger, L. D., Soares, V. Y., Deschler, D. G. and Stankovic, K. M. (2015). Secreted factors from
553 human vestibular schwannomas can cause cochlear damage. *Sci. Rep.* 5, 18599. doi: 10.1038/srep18599

554 Furness, D.N. (2015). Molecular basis of hair cell loss. *Cell Tissue Res.* 361, 387-399.

555 Granados, O. and Meza, G. (2005). Streptidine, a metabolic derivative produced after administration of
556 streptomycin in vivo, is vestibulotoxic in rats. *Histol. Histopathol*. 20, 357-364.

557 Greguske, E.A., Carreres-Pons, M., Cutillas, B., Boadas-Vaello, P. and Llorens, J. (2019) Calyx junction
558 dismantlement and synaptic uncoupling precede hair cell extrusion in the vestibular sensory epithelium
559 during sub-chronic 3,3'-iminodipropionitrile ototoxicity in the mouse. *Arch. Toxicol.* 93, 417-434.

560 Hasson, T., Gillespie, P.G., Garcia, J.A., MacDonald, R.B., Zhao, Y., Yee, A.G., Mooseker, M.S., Corey, D.P. (1997)
561 Unconventional myosins in inner-ear sensory epithelia. *J. Cell. Biol.* 137, 1287-1307.

562 Hirose, K., Westrum, L.E., Stone, J.S., Zirpel, L. and Rubel, E.W. (1999) Dynamic studies of ototoxicity in mature
563 avian auditory epithelium. *Ann. N.Y. Acad. Sci*. 884, 389-409.

564 Hirvonen, T.P., Minor, L.B., Hullar, T.E. and Carey, J.P. (2005). Effects of intratympanic gentamicin on vestibular
565 afferents and hair cells in the chinchilla. *J. Neurophysiol*. 93, 643-655.

566 Hunt, M.A., Miller, S.W., Nielson, H.C. and Horn, K.M. (1987) Intratympanic injections of sodium arsanilate
567 (atoxil) solution results in postural changes consistent with changes described for labyrinthectomized rats.
568 *Behav. Neurosci.* 101, 427–428.

569 Imamura, S., and Adams, J.C. (2003) Distribution of gentamicin in the guinea pig inner ear after local or systemic
570 application. *J. Assoc. Res. Otolaryngol.* 4, 176-195.

571 Jiang, H., Sha, S. H., Forge, A. and Schacht, J. (2006). Caspase-independent pathways of hair cell death induced
572 by kanamycin in vivo. *Cell Death Differ.* 13, 20–30.

573 Katsumi, S., Sahin, M. I., Lewis, R. M., Iyer, J. S., Landegger, L. D., & Stankovic, K. M. (2020). Intracochlear
574 perfusion of tumor necrosis factor-alpha induces sensorineural hearing loss and synaptic degeneration in
575 guinea pigs. *Front. Neurol.* 10, 1353.

576 Kohonen, A. and Tarkkanen, J. (1969) Cochlear damage from ototoxic antibiotics by intratympanic application.
577 *Acta Otolaryngol.* 68, 90-97.

578 Li, L., Nevill, G. and Forge, A. (1995). Two modes of hair cell loss from the vestibular sensory epithelia of the
579 guinea pig inner ear. *J. Comp. Neurol*. 355, 405-417.

580 Llorens, J. and Rodríguez-Farré, E. (1997). Comparison of behavioral, vestibular, and axonal effects of subchronic
581 IDPN in the rat. *Neurotoxicol. Teratol*. 19, 117-127.

582 Llorens, J., Demêmes, D. and Sans, A. (1993). The behavioral syndrome caused by 3,3'-iminodipropionitrile and
583 related nitriles in the rat is associated with degeneration of the vestibular sensory hair cells. *Toxicol. Appl.*
584 *Pharmacol.* 123, 199-210.

585 Lopez, I., Honrubia, V., Lee, S.C., Schoeman, G. and Beykirch, K. (1997) Quantification of the process of hair cell
586 loss and recovery in the chinchilla crista ampullaris after gentamicin treatment. *Int. J. Dev. Neurosci.* 15,
587 447-461.

588 Lopez-Escamez, J.A., Carey, J., Chung, W.H., Goebel, J.A., Magnusson, M., Mandala, M., Newman-Toker, D.E.,
589 Strupp, M., Suzuki, M., Trabalzini, F. and Bisdorff, A. (2015) Diagnostic criteria for Menière's disease. *J.*
590 *Vestib. Res.* 25, 1-7.

591 Lysakowski, A., Gaboyard-Niay, S., Calin-Jageman, I., Chatlani, S., Price, S.D. and Eatock, R.A. (2011). Molecular
592 microdomains in a sensory terminal, the vestibular calyx ending. *J. Neurosci*. 31, 10101–10114.

593 Maroto, A. F., Barrallo-Gimeno, A. and Llorens, J. (2021a). Relationship between vestibular hair cell loss and
594 deficits in two anti-gravity reflexes in the rat. Hear. Res. 410, 108336. doi: 10.1016/j.heares.2021.108336

595 Maroto, A.F., Greguske, E.A., Barrallo-Gimeno, A. and Llorens, J. (2021b) Evaluation of cellular and molecular
596 pathology in the rodent vestibular sensory epithelia by immunofluorescent staining and confocal
597 microscopy. In: E*xperimental Neurotoxicology Methods, Neuromethods, vol. 172*, Llorens, J. and Barenys.
598 M., Editors. Springer US, pp 35-50.

599 Maroto, A.F., Greguske, E.A., Deulofeu, M., Boadas-Vaello, P. and Llorens, J. (2021c) Behavioral assessment of
600 vestibular dysfunction in rats. In: E*xperimental Neurotoxicology Methods, Neuromethods, vol. 172*, Llorens,
601 J. and Barenys. M., Editors. Springer US, pp 199-215.

602 Martins-Lopes, V., Bellmunt, A., Greguske, E.A., Maroto, A.F., Boadas-Vaello, P. and Llorens, J. (2019)
603 Quantitative assessment of anti-gravity reflexes to evaluate vestibular dysfunction in rats. *J. Assoc. Res.*
604 *Otolaryngol.* 20, 553-563.

605 McInturff, S., Burns, J.C., Kelley, M.W. (2018) Characterization of spatial and temporal development of Type I
606 and Type II hair cells in the mouse utricle using new cell-type-specific markers. *Biol. Open* 7, bio038083.
607 doi: 10.1242/bio.038083.

608 Murillo-Cuesta, S., Contreras, J., Cediel, R. and Varela-Nieto, I. (2010) Comparison of different aminoglycoside
609 antibiotic treatments to refine ototoxicity studies in adult mice. *Lab. Anim.* 44, 124-131.

610 Nakagawa, T., Yamane, H., Shibata, S. and Nakai, Y. (1997) Gentamicin ototoxicity induced apoptosis of the
611 vestibular hair cells of guinea pigs. *Eur. Arch. Otorhinolaryngol.* 254, 9-14.

612 Nakayama, M., Riggs, L.C. and Matz, G.J. (1996) Quantitative study of vestibulotoxicity induced by gentamicin or
613 cisplatin in the guinea pig. *Laryngoscope* 106, 162-167.

614 Oesterle, E.C., Campbell, S., Taylor, R.R., Forge, A. and Hume, C.R. (2008) Sox2 and JAGGED1 expression in
615 normal and drug-damaged adult mouse inner ear. *J. Assoc. Res. Otolaryngol.* 9, 65-89.

616 Pellis, S.M., Pellis, V.C. and Teitelbaum, P. (1991) Labyrinthine and other supraspinal inhibitory controls over
617 head-and-body ventroflexion. *Behav. Brain Res*. 46, 99-102.

618 Rubel, E.W., Furrer, S.A. and Stone, J.S. (2013). A brief history of hair cell regeneration research and speculations
619 on the future. *Hear Res*. 297, 42-51.

620 Schirmer, M., Kaiser, A., Lessenich, A., Lindemann, S., Fedrowitz, M., Gernert, M. and Löscher, W. (2007).
621 Auditory and vestibular defects and behavioral alterations after neonatal administration of streptomycin to
622 Lewis rats: Similarities and differences to the circling (ci2/ci2) Lewis rat mutant. *Brain Res*. 1155, 179–195.

623 Sedó-Cabezón, L., Jedynak, P., Boadas-Vaello, P. and Llorens, J. (2015) Transient alteration of the vestibular
624 calyceal junction and synapse in response to chronic ototoxic insult in rats. *Dis. Model. Mech.* 8, 1323-1337.

625 Seoane, A., Demêmes, D. and Llorens, J. (2001a). Relationship between insult intensity and mode of hair cell loss
626 in the vestibular system of rats exposed to 3,3'-iminodipropionitrile. *J. Comp. Neurol.* 439, 385-399.

627 Seoane, A., Demêmes, D. and Llorens, J. (2001b). Pathology of the rat vestibular sensory epithelia during
628 subchronic 3,3'-iminodipropionitrile exposure: hair cells may not be the primary target of toxicity. *Acta*
629 *Neuropathol*. 102, 339-348.

630 Sousa, A.D., Andrade, L.R., Salles, F.T., Pillai, A.M., Buttermore, E.D., Bhat, M.A. and Kachar, B (2009). The
631 septate junction protein caspr is required for structural support and retention of KCNQ4 at calyceal synapses
632 of vestibular hair cells. *J. Neurosci*. 29, 3103-3108.

633 Sullivan, M. J., Rarey, K. E. and Conolly, R. B. (1987). Comparative ototoxicity of gentamicin in the guinea pig and
634 two strains of rats. Hear. Res. 31, 161–167.

635 Sultemeier, D. R. and Hoffman, L. F. (2017). Partial aminoglycoside lesions in vestibular epithelia reveal broad
636 sensory dysfunction associated with modest hair cell loss and afferent calyx retraction. Front. Cell. Neuorsci.
637 11, 331.

638 Taylor, R.R., Nevill, G. and Forge, A. (2008) Rapid hair cell loss: a mouse model for cochlear lesions. *J. Assoc. Res.*
639 *Otolaryngol.* 9, 44-64.

640 von Brevern, M., Bertholon, P., Brandt, T., Fife, T., Imai, T., Nuti, D. and Newman-Toker, D. (2015) Benign
641 paroxysmal positional vertigo: Diagnostic criteria. *J. Vestib. Res.* 25, 105-117-

642 Wu, W.J., Sha, S.H., McLaren, J.D., Kawamoto, K., Raphael, Y. and Schacht, J. (2001) Aminoglycoside ototoxicity
643 in adult CBA, C57BL and BALB mice and the Sprague-Dawley rat. *Hear. Res.* 158; 165-178.

644 LEGENDS FOR FIGURES

645 **Figure 1.** Effects of sub-chronic streptomycin on the tail-lift reflex of rats. Data are mean ± SE minimum angles
646 formed by the nose, the back of the neck, and the base of the tail during the reflex behaviour elicited by a tail-
647 lift manoeuvre. Loss of vestibular function causes loss of the anti-gravity trunk extension reflex, which results in
648 ventral curling and thus in smaller angles. **A.** Effects of one injection per day at 0 (CTRL, vehicle control) or 500
649 mg/kg (STR-500) of streptomycin for 6 weeks, starting at 21 days of age. * $p<0.05$, different from control group
650 after significant day by treatment interaction effect in repeated-measures MANOVA. **B.** Effects of two injections
651 per day at 0 (CTRL, vehicle control), 300 (STR-300x2), 350 (STR-350x2), or 400 (STR-400x2) mg/kg of
652 streptomycin for 6, 6, 4, or 3 weeks, respectively, starting at 21 days of age. The numbers of animals were
653 reduced to 6 in the CTRL group after day 28, and to 7 in the STR-300x2 and STR-350x2 groups after day 21. **a, b,**
654 **c, d**: groups with different letters are significantly different ($p<0.05$), Duncan's test after significant ANOVA on
655 that day. **C.** Recuperation of the tail-lift reflex after the end of exposure in rats administered once a day with 500
656 mg/kg (STR-500) of streptomycin for 6 weeks. **D.** Loss and recuperation of the tail-lift reflex in two individual rats
657 administered twice a day with 350 (STR-350) or 400 mg/kg (STR-400) of streptomycin for 3 weeks, followed by 3
658 weeks of recovery.

659 **Figure 2.** Effects of sub-chronic streptomycin on the vestibular sensory epithelium of the rat as observed in
660 surface preparations of saccules examined by SEM. **A.** Control saccule, showing a high and uniform density of
661 stereocilia bundles throughout the macula. **B.** Effect of one injection per day of 500 mg/kg of streptomycin (STR-
662 500) for 8 weeks. A reduced density of stereocilia bundles is noticeable at this low magnification. The boxed area
663 is shown at higher magnification in panel C. **C.** Higher magnification of the saccule shown in panel B. Note the
664 areas where the lack of stereocilia bundles is evident (arrows). **D and E.** High magnification views of a saccule
665 from a STR-500 rat at 6 weeks of treatment. Note the contacts between the apical edges of supporting cells,
666 marked by a high density of microvellosities, denoting the lack of stereocilia bundles (star), and the bundles

667 showing stereocilia fusion and HC protrusion into the luminal cavity (arrows). **Scale Bars:** 100 μm in **A** and **B**; 20
668 μm in **C**; 2 μm in **D**; 5 μm in **E**.

669 **Figure 3.** Effect of sub-chronic streptomycin on the numbers of HCI and HCII in the vestibular epithelia of the rat.
670 **A, B, C**. Effect of 500 mg/kg of streptomycin, once a day, for 6 or 8 weeks, as recorded at the end of the
671 exposure period or at the end of a recovery period of 8 weeks after treatment. Vestibular cristae, utricles and
672 saccules were immunolabelled with anti-MYO7A (red, to label all HCs), anti-CASPR1 (green, to identify HCI) and
673 anti-calretinin (blue, to label HCII) antibodies, and examined by confocal microscopy. The central/striola and
674 peripheral regions of the epithelia were evaluated separately. **A**. Representative images from the peripheral
675 utricle of a vehicle control rat, a rat treated with streptomycin for 8 weeks (STR-500 8wk), and a recovery (STR-
676 500 R) rat. HCI were defined by MYO7A+ cells with adjacent CASPR1 label, even if thin or fragmented, and no
677 calterinin label (arrows). Note the fragmentation of the CASPR1 label in the STR-500 (8wk) rat. **Scale bar**: 20 μm.
678 **B and C.** Counts of HCI **(B)** and HCII **(C)** cells. Data are mean number of cells +/- SE per section. For each animal
679 and epithelial zone, numbers were obtained by averaging counts from 8 confocal stacks from a representative
680 histological section. **D, E**. Effect of 300 (STR-300x2), 350 (STR-350x2) or 400 (STR-400x2) mg/kg of streptomycin,
681 twice a day, for 6, 4, or 3 weeks. The recovery (R) group includes animals allowed 3 weeks of recovery after
682 receiving STR-350x2 or STR-400x2 for 3 or 4 weeks. Vestibular cristae were labelled with anti-SPP1 (blue, to label
683 HCI), anti-CASPR1 (green) and anti-calretinin (red) antibodies. HCI were defined as SPP1+ cells and HCII were
684 cells with calretinin label. **D.** Partial view of representative sections of control and streptomycin cristae. **Scale**
685 **bar**: 20 μm. **E.** Relative numbers of HCI and HCII in the crista sections. Data are mean number of cells +/- SE per
686 transversal section, including central and peripheral regions. In **B**, **C**, and **E**, the number of replicas in the figure
687 legends indicate minimum/maximum number of animals counted per epithelium and zone in the treatment
688 group. **a, b, c, ab**: groups not sharing a letter are different ($p<0.05$), Duncan's multiple-comparisons test after
689 significant ($p<0.05$) one-way ANOVA. **(n.s.):** non-significant ($p>0.05$) group differences in the ANOVA analysis.

690 **Figure 4.** Effects of sub-chronic streptomycin on the expression of CASPR1 in the central/striola (C/S) and
691 peripheral (P) regions of the vestibular crista, utricle and saccule of the rat. The samples were labelled with anti-
692 MYO7A (red), anti-CASPR1 (green) and anti-calretinin (blue) antibodies. **A.** Representative images from mid-
693 crista sections from a CTRL rat (**a** to **d**), a rat treated with 500 mg/kg of streptomycin, once a day, for 6 weeks (**e**
694 to **h**), and a rat allowed a recovery period of 10 weeks after the streptomycin treatment (**i** to **l**). Note the loss
695 and fragmentation of the CASPR1 label caused by streptomycin and its recuperation after recovery. The
696 intensity of MYO7A label also decreased and recovered. **B.** Quantitative analysis of the CASPR1 fluorescence.
697 Data are normalised arbitrary fluorescence amount per cell +/- SE. For each animal, epithelium and zone, the
698 average amount of fluorescence was obtained from all HCs available for analysis up to 40 cells. Numbers below
699 the bars indicate number of animals included per group. **a, b**: groups not sharing a letter are different ($p<0.05$),
700 Duncan's multiple-comparisons test after significant ($p<0.05$) one-way ANOVA.

701 **Figure 5.** Effects of sub-chronic streptomycin on the expression of synaptic proteins in the HCI and calyx
702 afferents of the rat. **A.** Redistribution of KCNQ4 in the inner and outer membranes of the calyx terminals
703 afferent to HCI. Vestibular crista were labelled with anti-CASPR1 (green) and anti-KCNQ4 (red) antibodies. The
704 asterisk indicates a calyx with a control-like co-localisation of CASPR1 and KCNQ4 in the inner membrane of the
705 calyx. The arrowhead points to a calyx with CASPR1 loss and reduced co-localisation, with the KCNQ4 antibody
706 labelling a greater area than the CASPR1 antibody. The arrow points to the outer membrane of a calyx with
707 greatly reduced CASPR1 label and redistribution of KCNQ4 throughout both the inner (i and i') and outer (o and
708 o') membranes. **B.** Quantitative analysis of the distribution of KCNQ4 label in the inner and outer face of the
709 calyces in crista from control rats (CTRL), rats treated with 500 mg/kg of streptomycin (STR-500), once a day, for
710 6 or 8 weeks, and rats allowed a recovery period of 8-10 weeks after the streptomycin treatment. Note that
711 control and recovery animals do not display KCNQ4 in the outer face membrane. Data are mean arbitrary
712 fluorescence units +/- SE. The number of replicas indicate the number of animals included in the analysis per
713 group. **a, b**: groups not sharing a letter are different ($p<0.05$), Duncan's multiple-comparisons test after

714 significant ($p<0.05$) one-way ANOVA. **C.** Labelling of pre-synaptic (Ribeye, red) and post-synaptic (PSD-95, green)
715 proteins on HCs (MYO7A, white) in vestibular crista. In subpanel **c1**, the MYO7A label is included to show HC
716 bodies in a control crista. Subpanel **c2** shows the same image without the MYO7A label but including lines
717 delineating the limits of two HCs and arrows pointing to examples of pairs of ribeye and PSD-95 puncta. **D.**
718 Effects of sub-chronic streptomycin on the numbers of synaptic puncta per 2.7 μm-tick optical sections of HCs.
719 Data are mean number of pre-synaptic and post-synaptic puncta, as well as pre- and post-synaptic pairs (Co-
720 localization), +/- SE, from control rats (CTRL) and rats treated with 500 mg/kg of streptomycin (STR-500), once a
721 day, for 6 weeks. The number of replicas indicate the number of animals included in the analysis per group. *: $p<$
722 0.05, and ***: $p<0.001$, CTRL versus STR-500, Student's T-test.

723 **Figure 6.** Effects of sub-chronic streptomycin on the calyceal junction and calyx integrity as observed by TEM. **A.**
724 Control crista. The calyceal junction is revealed by the high electron density of the apposing membranes (long
725 arrows) of HCI and inner side of the calyx (c), higher than that found in the outer side of the calyx (arrowheads).
726 **B.** Crista of a rat exposed to 500 mg/kg of streptomycin, once a day, for 6 weeks. In most of the area where the
727 calyceal junction should be found, the apposing membranes show a low electron density (short arrows), similar
728 to that in the outer face of the calyx (arrowhead). **C.** Higher magnification of the calyceal junction (long arrow)
729 and the outer side of the calyx (arrowhead) in a control saccule. **D.** Higher magnification from a crista of a rat
730 exposed to 500 mg/kg of streptomycin, once a day, for 6 weeks. Note the short segment of calyceal junction
731 (long arrow) that remains together with areas devoid of it (short arrow) and the similarity between the latter
732 and the membranes in the outer side of the calyx (arrowheads). **E.** Calyceal junction dismantlement and calyx
733 fragmentation in a HCI showing evidence of ongoing extrusion, from a utricle of a rat exposed to 300 mg/kg of
734 streptomycin, twice a day, for 6 weeks. Note the absence of calyceal junction (short arrows), the fragmentation
735 of the calyx (c, green shadow), and the direct contact between supporting cells and the HCI (stars). The purple
736 shadow highlights one supporting cell (sc). **F.** Higher magnification of the boxed area in panel **E**. Note the
737 similarity of the membranes between the place where the calyceal junction is missing (short arrows) and the

738 outer side of the calyx (arrowheads). Note also the direct contact between a supporting cell (sc) and the HCI
739 (star). **Scale Bars: A**, **B**, and **E**, 2 mm; **C**, **D**, and **F**, 1 mm.

740 **Figure 7.** Evidence of HC extrusion in utricles of rats exposed to sub-chronic streptomycin as observed by
741 immunofluorescence and TEM. The images are from rats administered twice a day with 350 mg/kg of
742 streptomycin for 4 weeks, or with 300 mg/kg for 6 weeks. **A.** Utricles immunolabelled with antibodies against
743 MYO7A (red), CASPR1 (green) and radixin (blue). The radixin label of stereocilia and microvilli outlines the
744 surface of the epithelium. Arrowheads point to HCs protruding (**a**, **b**), extruding (**c**, **d**, **e**) or completely extruded
745 (**f**) into the luminal cavity of the utricle. **B** and **C.** TEM images of HCs in a protrusion stage corresponding to that
746 shown in panels **a** and **b**, respectively, of part **A**. Stereocilia (arrows) and striated organelles (arrowheads)
747 identify the extruding cells as HCs. In **B**, note the position of the nucleus of the HC inside the epithelium, and the
748 remnant of a calyx terminal (green shadow) that identifies the HC as a HCI. In **C**, note the position of the nucleus
749 of the HC (unidentified type), half way into the luminal cavity of the utricle. **Scale Bars: A**, 20 mm; **B**, and **C**, 2
750 mm.

751 **Figure 8.** Evaluation of the calyceal junction in vestibular epithelia from patients of vestibular diseases, as
752 revealed by CASPR1 immunolabel (green, light blue when co-localizing with calretinin blue label). In the main
753 panels, HC bodies are labelled with an anti-MYO7A antibody (red). Calretinin is shown in blue in main panels **C** to
754 **F**, and in purple in the inset in **C**. **A**. Epithelium from a patient of Ménière's Disease showing no pathological
755 features. Note the elevated density of HCs and the continuous distribution of the CASPR1 label throughout the
756 calyceal junction area of each HCI. **B.** Epithelium from a meningioma patient, showing also no overt pathology.
757 **C.** Epithelium from a meningioma patient. Note the low density of HCs and the normally continuous CASPR1
758 label in calyces of both calretinin+ calyx-only terminals (arrowhead) and calretinin- dimorphic terminals (short
759 arrow). The **inset** displays the same two calyces; a thinner stack is shown to highlight the uninterrupted CASPR1
760 label and its placement in the inner membrane of the calretinin+ calyx of the calyx-only terminal. **D.** Utricle
761 periphery from a vestibular schwannoma patient. Around different HCI, the calyceal CASPR1 label is found in

762 both normal continuous distribution (arrowhead) and in faint and broken distribution (long arrows). **E.** Striola
763 region of the same utricle in **D**. Although some calyceal junctions display a roughly normal continuous
764 distribution of the CASPR1 label (arrowheads), most display faint, broken or largely absent label (arrows). **F**.
765 Higher magnification image from the same patient in **D** and **E.** Two calyces formed by calyx-only terminals are
766 highlighted, one with continuous CASPR1 label (arrowhead) and the other with a patched distribution of this
767 label (long arrow). **G.** Epithelium from a different vestibular schwannoma patient displaying normal CASPR1
768 distribution in calyces from dimorphic terminals (arrowhead) and a double calyx of a calretinin+ calyx-only
769 terminal displaying a partial CASPR1 label in one HC (short arrow) and no CASPR1 in the other HC (long arrow).
770 **Image thickness: A**, 12 μm; **B**, 10 μm; **C**, main 9.5 μm, inset 5 μm; **D**, 1.6 μm; **E**, 2.6 μm; **F**, 5 μm; **G**, 6 μm. **Scale**
771 **Bars: A**, **C**, **D**, and **E**, 25 μm; **B**, 50 μm; **F**, and **G**, 5 μm.

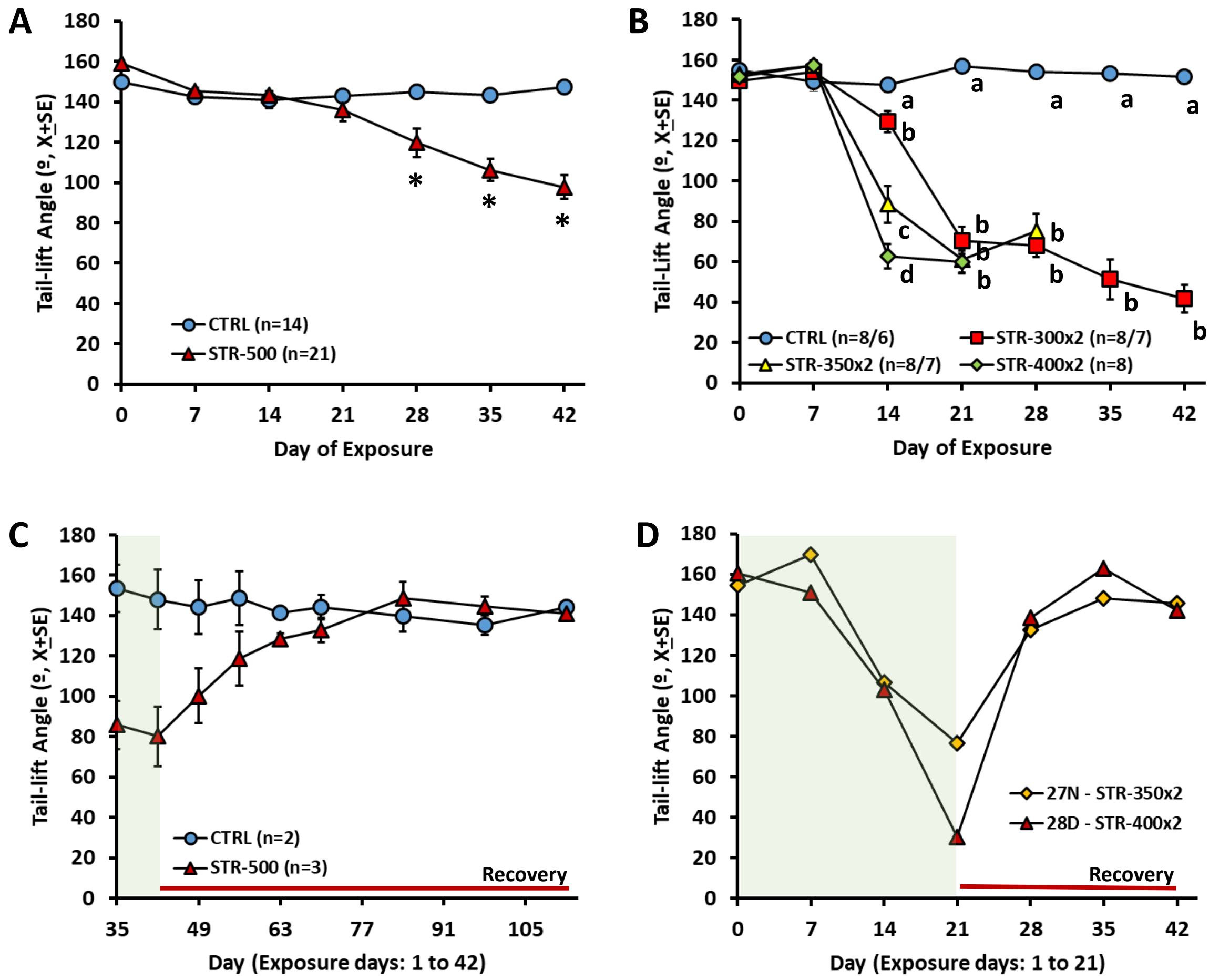
A
Tail-lift Angle (º, X+SE)
Day of Exposure
CTRL (n=14)
STR-500 (n=21)
B
Tail-Lift Angle (º, X+SE)
Day of Exposure
CTRL (n=8/6)
STR-300x2 (n=8/7)
STR-350x2 (n=8/7)
STR-400x2 (n=8)
C
Tail-lift Angle (º, X+SE)
Day (Exposure days: 1 to 42)
CTRL (n=2)
STR-500 (n=3)
Recovery
D
Tail-lift Angle (º, X+SE)
Day (Exposure days: 1 to 21)
27N - STR-350x2
28D - STR-400x2
Recovery

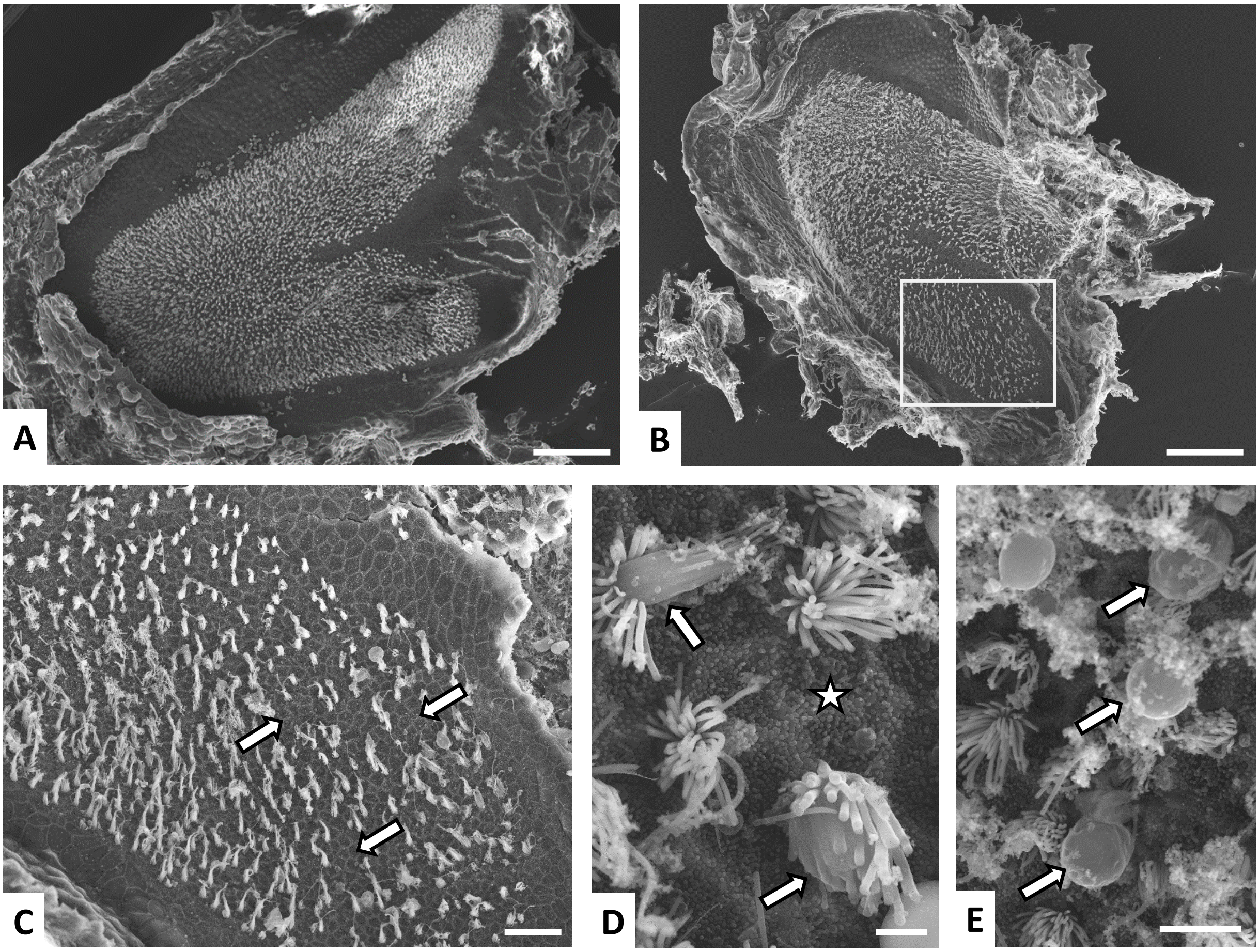
A
B
C
D
E

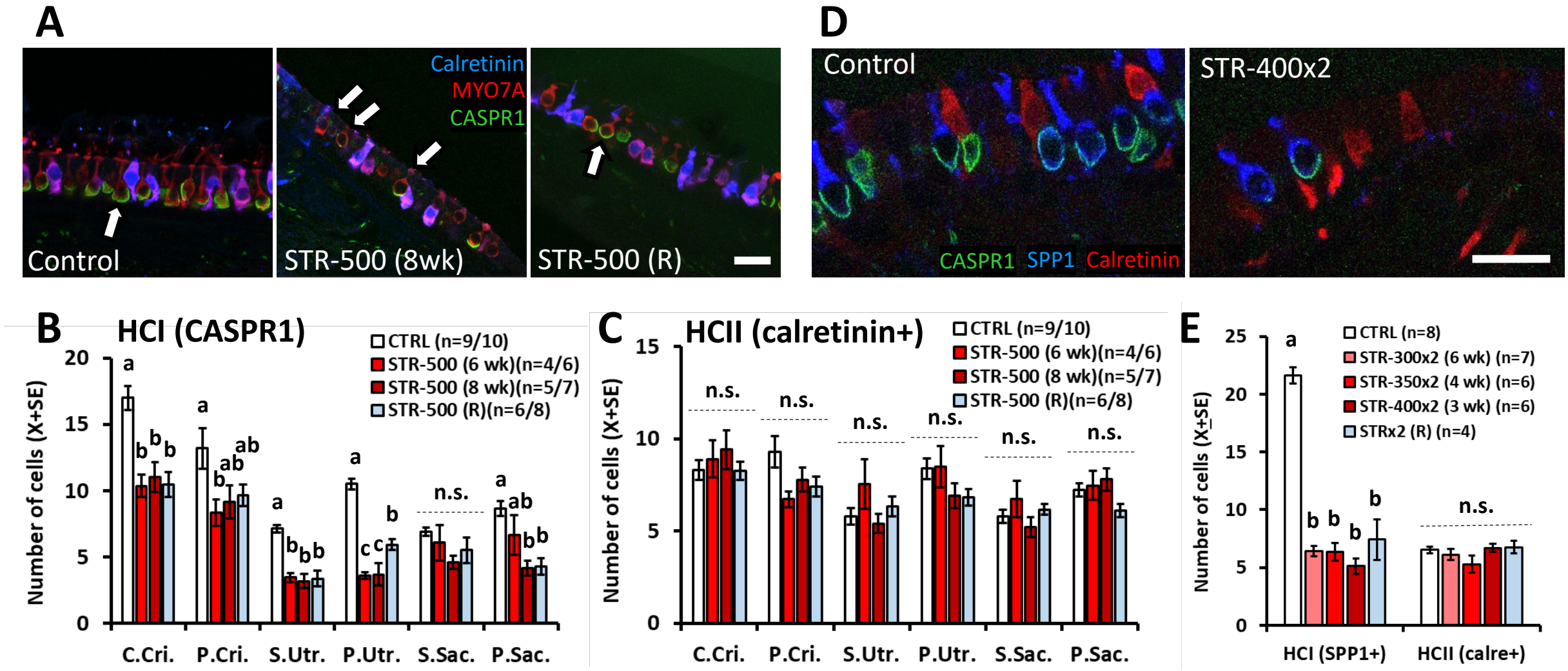
A
Calretinin
MYO7A
CASPR1
Control
STR-500 (8wk)
STR-500 (R)
D
Control
STR-400x2
CASPR1
SPP1
Calretinin
B
HCI (CASPR1)
CTRL (n=9/10)
STR-500 (6 wk)(n=4/6)
STR-500 (8 wk)(n=5/7)
STR-500 (R)(n=6/8)
Number of cells (X+SE)
C.Cri.
P.Cri.
S.Utr.
P.Utr.
S.Sac.
P.Sac.
n.s.
C
HCII (calretinin+)
E
CTRL (n=8)
STR-300x2 (6 wk) (n=7)
STR-350x2 (4 wk) (n=6)
STR-400x2 (3 wk) (n=6)
STRx2 (R) (n=4)
HCI (SPP1+)
HCII (calre+)

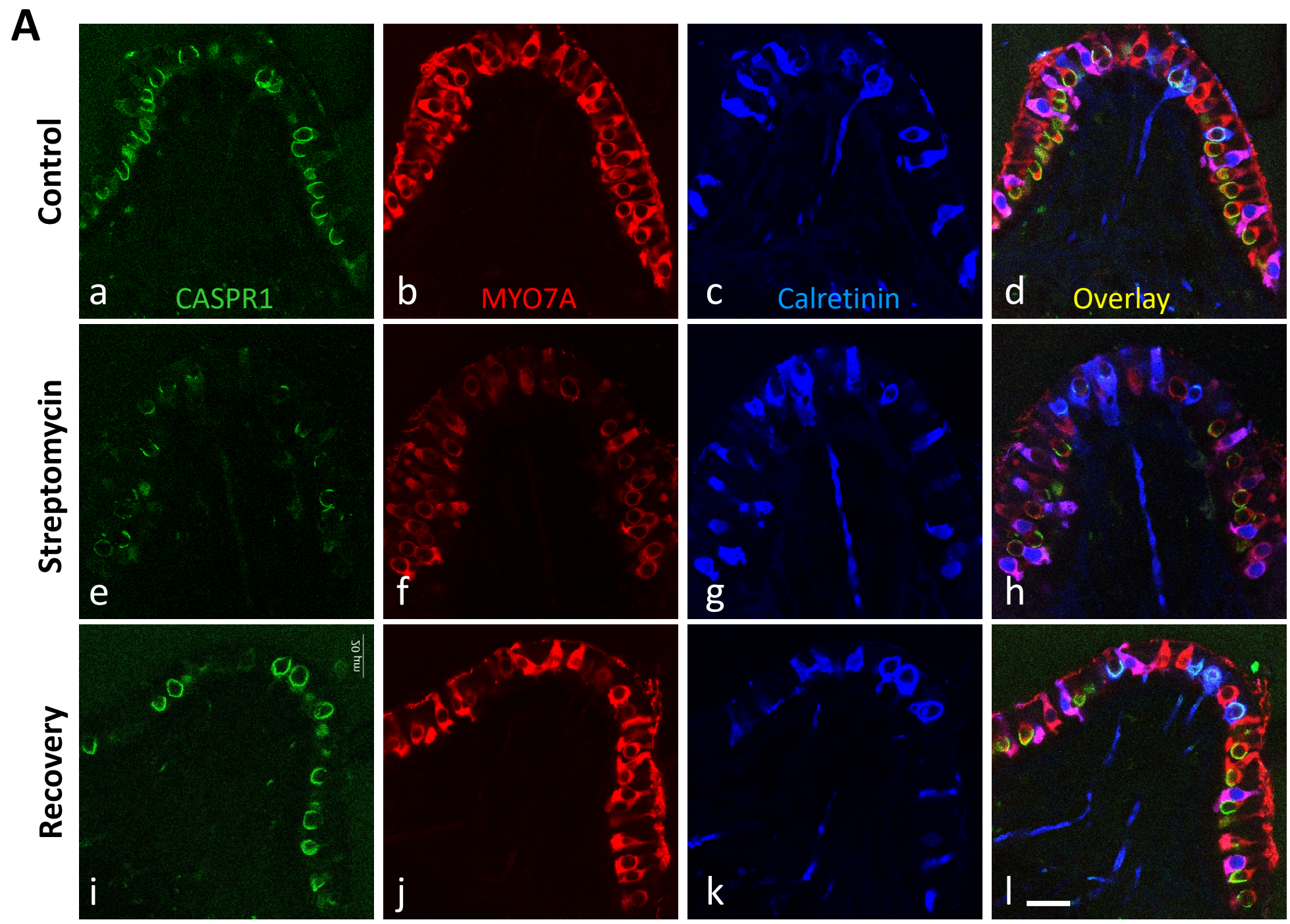
A
Control
Streptomycin
Recovery
a
CASPR1
b
MYO7A
c
Calretinin
d
Overlay
e
f
g
h
i
j
k
l
20 µm

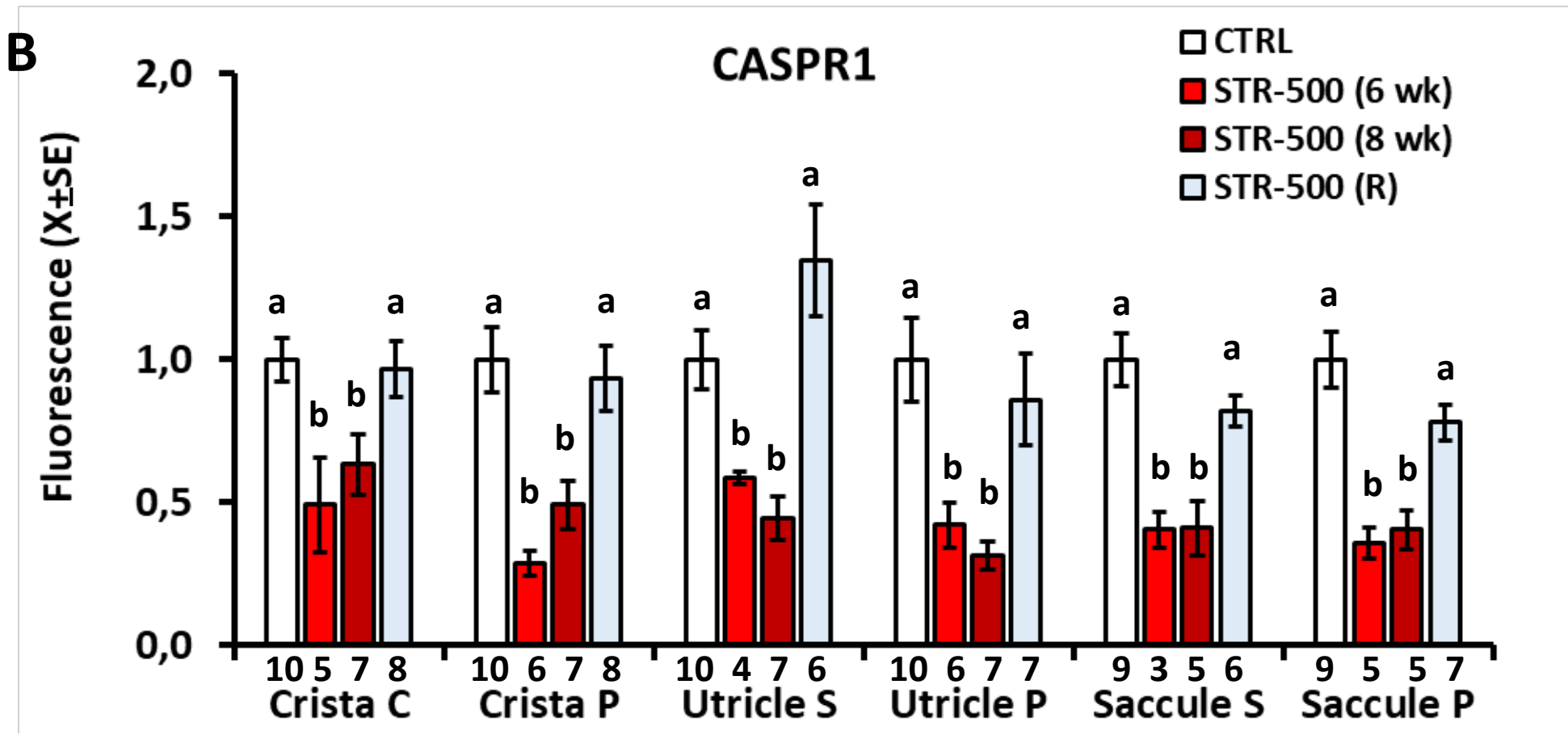
B
CASPR1
CTRL
STR-500 (6 wk)
STR-500 (8 wk)
STR-500 (R)
Fluorescence (X±SE)
2,0
1,5
1,0
0,5
0,0
10 5 7 8
10 6 7 8
10 4 7 6
10 6 7 7
9 3 5 6
9 5 5 7
Crista C
Crista P
Utricle S
Utricle P
Saccule S
Saccule P

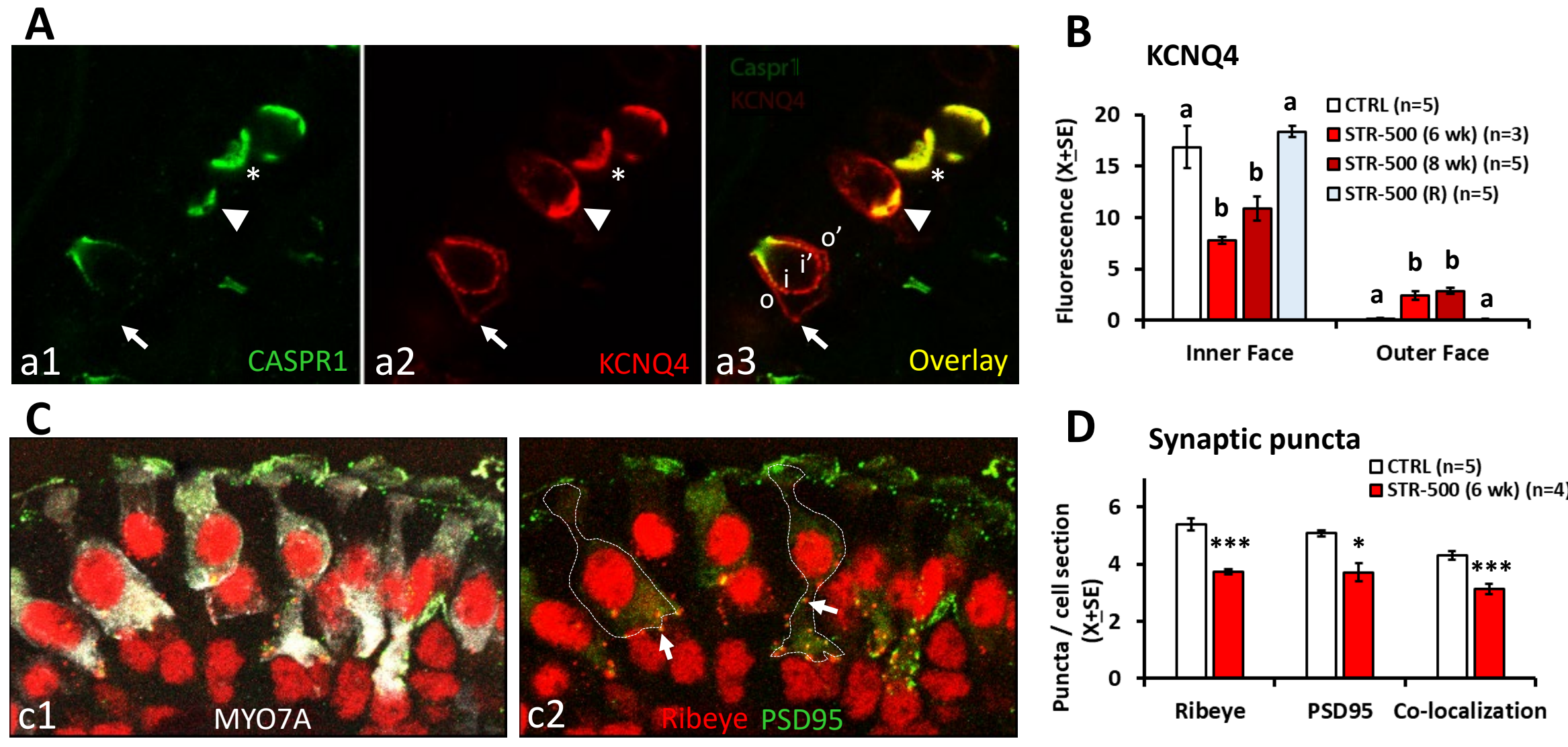
A
a1
CASPR1
a2
KCNQ4
a3
Overlay
Caspr1
KCNQ4
o'
i'
i
o
B
KCNQ4
Fluorescence (X±SE)
CTRL (n=5)
STR-500 (6 wk) (n=3)
STR-500 (8 wk) (n=5)
STR-500 (R) (n=5)
Inner Face
Outer Face
C
c1
MYO7A
c2
Ribeye
PSD95
D
Synaptic puncta
CTRL (n=5)
STR-500 (6 wk) (n=4)
Puncta / cell section (X±SE)
Ribeye
PSD95
Co-localization

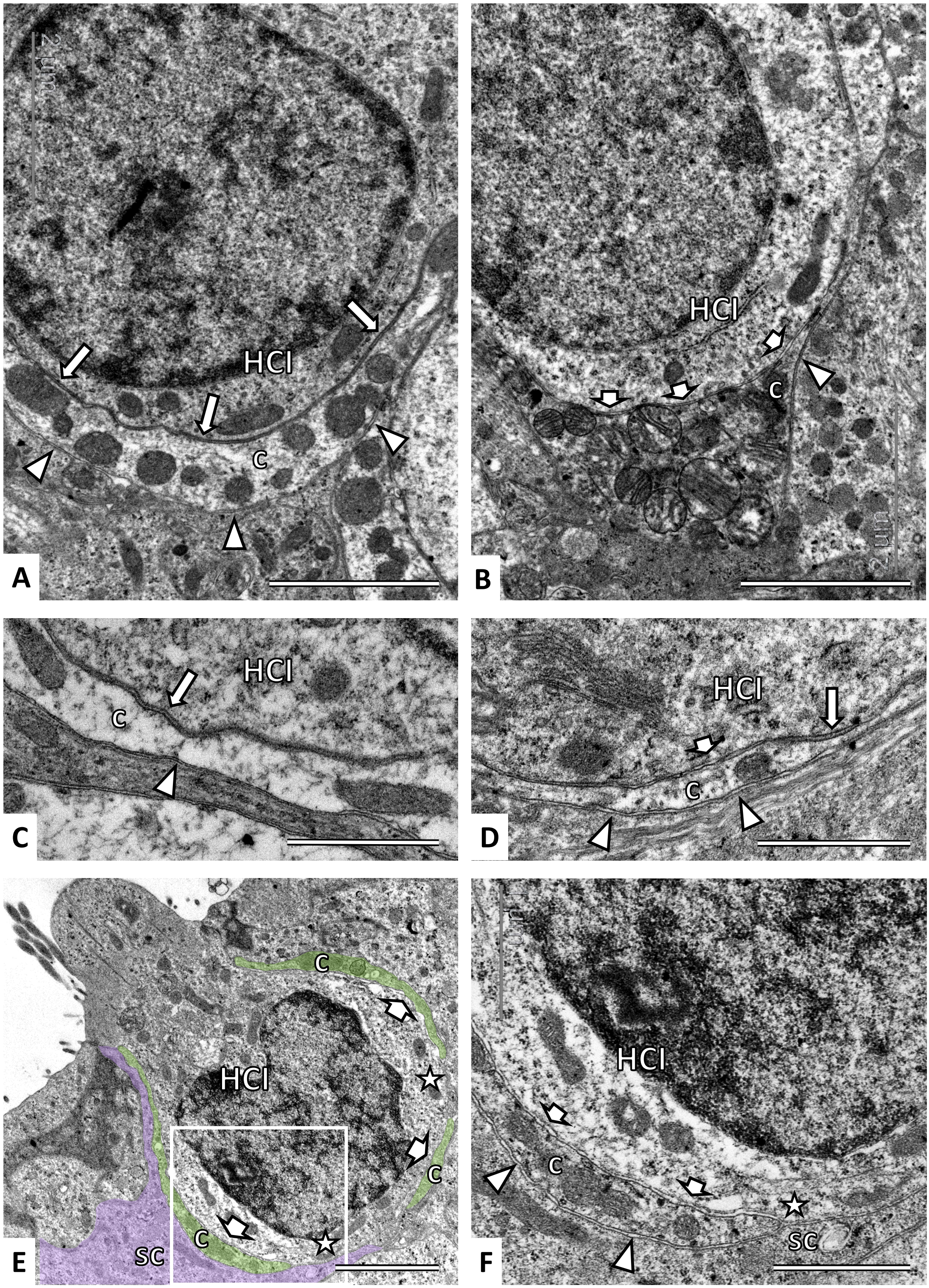
A
HCI
C
2 µm
B
HCI
C
2 µm
C
HCI
C
D
HCI
C
E
HCI
C
C
C
SC
F
HCI
C
SC

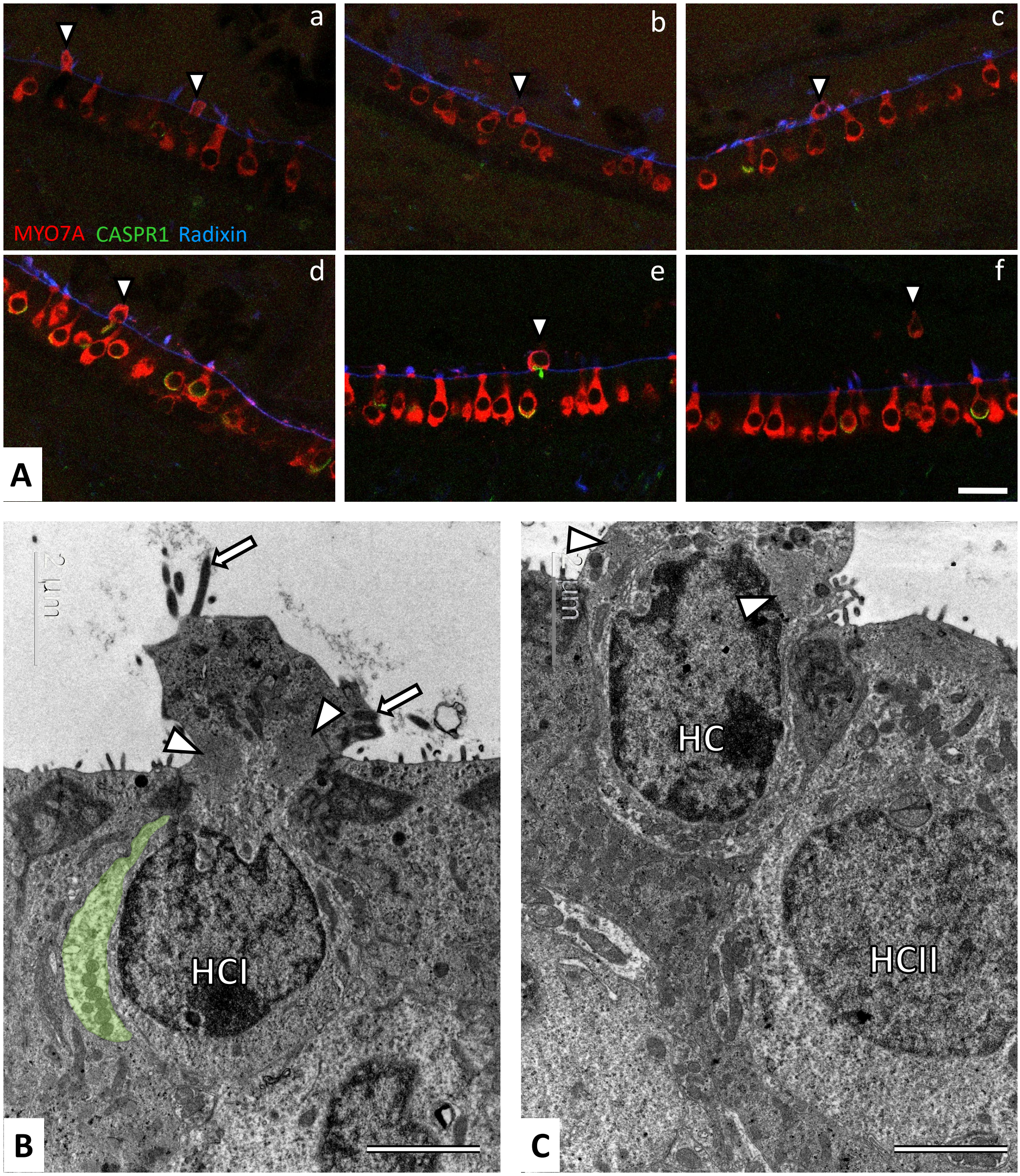
a
b
c
d
e
f
MYO7A CASPR1 Radixin
A
2 µm
HCI
B
3 µm
HC
HCII
C

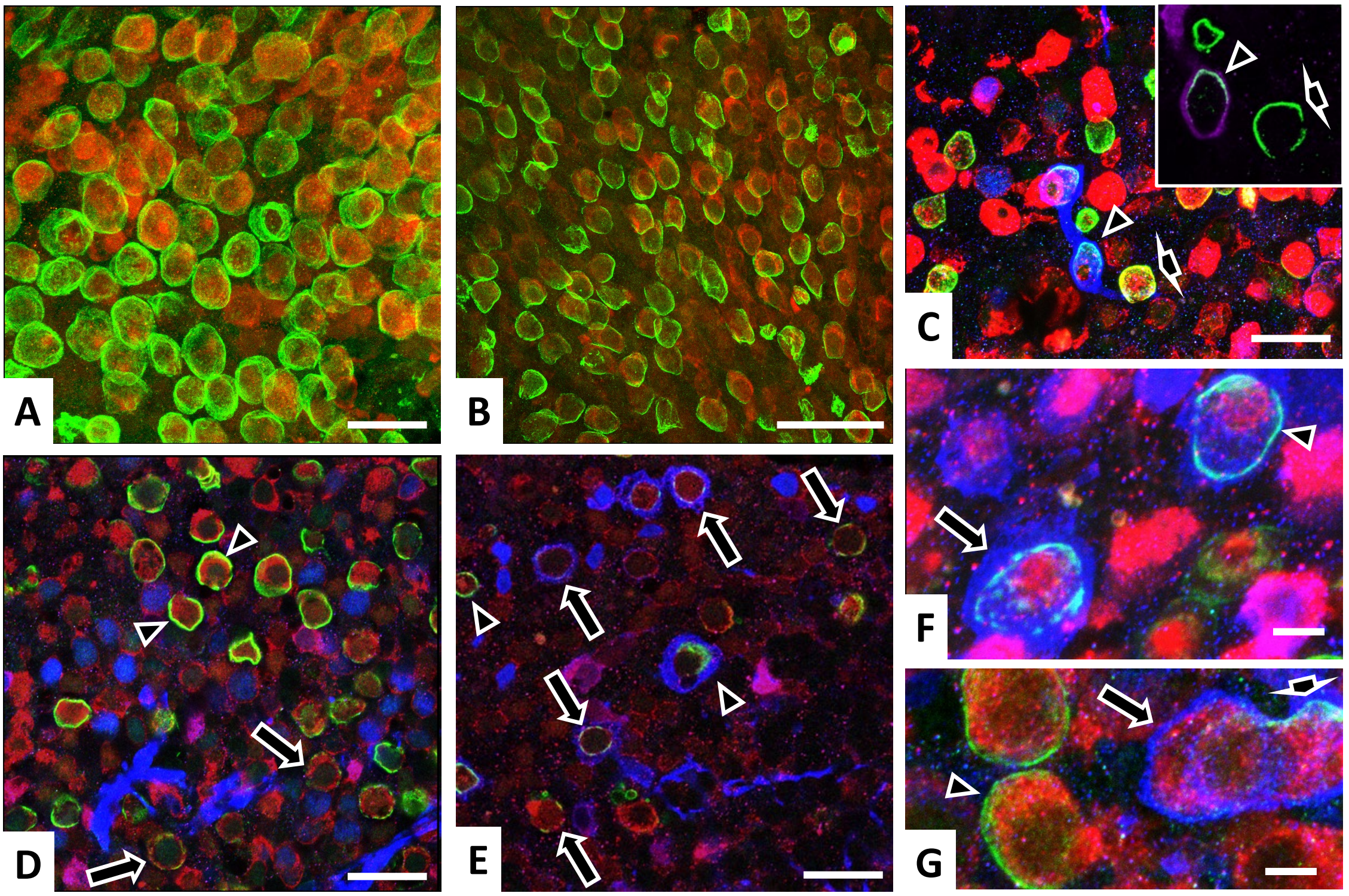
A
B
C
D
E
F
G